Geothermal Energy

RESEARCH Open Access

Water–rock interactions in the Bruchsal geothermal system by U–Th series radionuclides

Lena Kölbel[1*], Thomas Kölbel[2], Ulrich Maier[1], Martin Sauter[1], Thorsten Schäfer[3] and Bettina Wiegand[1]

*Correspondence: lkoelbel@geo.uni-goettingen.de
[1] Department of Applied Geology, Geoscience Centre, University of Göttingen, Goldschmidtstr. 3, 37077 Göttingen, Germany
Full list of author information is available at the end of the article

Abstract

Uranium and thorium decay series disequilibria in deep geothermal brines are a result of water–rock interaction processes. The migratory behavior of radionuclides provides valuable site-specific information and can therefore be an important tool for reservoir characterization and sustainable management of geothermal sites. In this study, we present data from long-term monitoring of naturally occurring ^{238}U, ^{232}Th and ^{235}U series radionuclides analyzed in brine samples collected from the Permo-Triassic sedimentary reservoir rock at the Bruchsal geothermal site (SW Germany). The results show that radionuclides of the elements radium (^{226}Ra, ^{228}Ra, ^{224}Ra, ^{223}Ra), radon (^{222}Rn), and lead (^{210}Pb, ^{212}Pb) are rather soluble in brine, while isotopes of uranium (^{238}U, ^{234}U, ^{235}U), thorium (^{232}Th, ^{228}Th, ^{230}Th), polonium (^{210}Po), and actinium (^{227}Ac, ^{228}Ac) have low solubilities and are mostly immobile. Activities of radium isotopes in the geothermal brine exceed those of their thorium progenitors (average ^{226}Ra = 29.9 Bq kg^{-1}, about 10^3 times that of its ^{230}Th parent). Modelling the observed disequilibria allows the following conclusion on water–rock interaction processes: (1) supply from alpha-recoil depends on isotope half-life because it is limited by the rate of diffusion through microfractures causing isotopic fractionation. (2) Radium retardation due to adsorption is low (^{226}Ra/^{222}Rn = 1.3) resulting in adsorption–desorption rate constants in the order of 10^{-10} s^{-1} for k_1 and 10^{-9} for k_2. (3) Scavenging of ^{226}Ra from brine can best be explained by co-precipitation with barite resulting in an observed ^{226}Ra anomaly in the solids of the reservoir section. The precipitation rate constant amounts to ca. 3.4×10^{-8} s^{-1} corresponding to a mean removal time of radium from brine by mineral precipitation to approximately 1 year.

Keywords: Geothermal brine, Naturally occurring radionuclides, Water–rock interaction processes, Upper Rhine Graben

Introduction

In geothermal brines, activities of naturally occurring radionuclides are controlled by a number of processes including radioactive decay and production, recoil supply, adsorption–desorption, and precipitation–dissolution.

The natural decay chains of ^{238}U, ^{232}Th and ^{235}U comprise elements with different hydrogeochemical properties and with more than one isotope (Fig. 1). While in closed systems all daughter nuclides will achieve secular radioactive equilibrium with respect to their parent nuclides (daughter/parent activity ratio becomes unity), deep geothermal

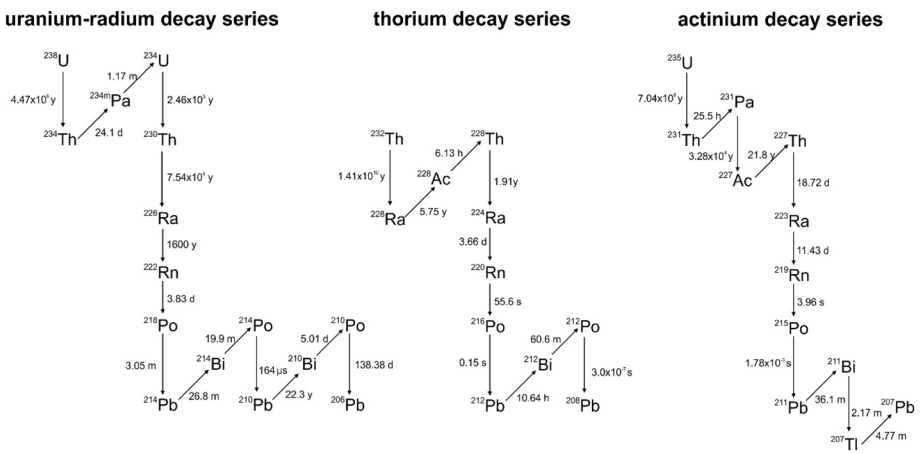

Fig. 1 Uranium–radium, thorium and actinium decay series. Vertical arrows indicate alpha decay, diagonal arrows indicate beta decay. For radionuclides with more than one decay mode, only the most frequently occurring is given

brines interact with solid phases with whom they come into contact. In consequence of these water–rock interactions, an elemental fractionation occurs resulting in a state of disequilibria (Osmond and Cowart 1992). Such radioactive disequilibria were found in deep geothermal brines in the Upper Rhine Graben (URG). Here, radium isotopes (^{228}Ra, ^{226}Ra, ^{224}Ra, ^{223}Ra) have activities far exceeding those of their thorium progenitors (Eggeling et al. 2013). Radioactive disequilibria caused by the preferred solution of radium were also documented for deep geothermal brines in the Salton Sea Geothermal field (Zukin et al. 1987). Previous studies have shown that radium concentrations are often high in saline waters (Kraemer and Reid 1984; Dickson 1985) and geothermal brines (Hammond et al. 1988; Rihs and Condomines 2002; Condomines et al. 2012), but rather low in low-temperature, low-salinity groundwaters (Krishnaswami et al. 1982; Luo et al. 2000; Porcelli 2008).

Modelling of these disequilibria provides information about the respective water–rock interaction processes controlling radionuclide supply into and scavenging from solution, respectively. This information is very useful to investigate the long-term migratory behavior of uranium and thorium series radionuclides which is not only an important issue for the integrity of nuclear waste disposals, but also for geothermal sites in terms of handling radionuclide-bearing precipitated minerals (scales) in surface installations: natural radionuclides which are once mobilized by water–rock interaction processes in the reservoir may be transported with the fluid through the geothermal power plant and trapped in solid solutions because of changing temperature and pressure conditions. Furthermore, understanding the migratory behavior of radionuclides in the reservoir may be useful for the characterization and sustainable management of the geothermal reservoir.

Tricca et al. (2001) describe the water–rock interactions as physico-chemical reactions between three phases: the aqueous phase, the solid minerals and a reactive surface layer with specific properties, area and thickness. The transfer rate of a radionuclide from the rock material into solution depends on: (a) the in situ radioactive decay of its dissolved

parent; (b) the desorption from the surface coating; (c) the alpha-recoil across the solid–liquid interface within a distance of several tens of nanometers, and (d) the dissolution of the aquifer solid. The removal of a radionuclide from the brine depends on: (a) its radioactive decay in solution; (b) the adsorption onto the surface layer, and (c) the incorporation into precipitates.

In the past, several mathematical solutions of simplified aquifer models dealing with naturally occurring radionuclides have been developed. Andrews et al. (1982, 1989) considered physico-chemical mechanisms for radionuclide supply and removal and calculated the timescale of water–rock interactions. However, the authors did not consider transport by advection. Krishnaswami et al. (1982) computed rate constants of sorption processes. Furthermore, they determined residence times of daughter nuclides by means of alpha-recoil input from ^{222}Rn activities, although without considering the effects of advective transport and mineral dissolution/precipitation. Davidson and Dickson (1986) suggested a model of uranium and radium isotopes transport including dispersive flow, but without considering precipitation and dissolution processes. Ku et al. (1992) proposed a model that accounts for radionuclide transport by advection and first-order kinetics, sorption–desorption, dissolution–precipitation of U–Th series radionuclides processes as well as the supply from alpha-recoil. Tricca et al. (2000, 2001) suggested a model for the combined groundwater transport of naturally occurring U, Th, Ra, and Rn isotopes with regard to advective transport as well as the physico-chemical processes of weathering, decay, alpha-recoil and sorption at the water–rock interface.

The present study is aimed at better understanding of the behavior of uranium and thorium series radionuclides in the Bruchsal geothermal brine. A comprehensive dataset was generated by frequent, long-term fluid sampling. Results of the geochemical surveys of major/minor elements as well as isotopic measurements of U, Th, Ac, Ra, Rn, Po, Bi and Pb are presented below. From the observed isotope disequilibria, water–rock interactions were investigated and their effects on radionuclide transport in the geothermal reservoir assessed. Since the modelling of radioactive disequilibria requires both types of information, the composition of the fluid and the solid phase, the authors refer to their previous work (Kölbel et al. 2020) where the Bruchsal reservoir rock was intensively examined based on cuttings from the geothermal boreholes. The modelling part of this study focuses on radium isotopes since their range in half-lives and their interrelation in the respective decay chain (cf. Fig. 1) allows the determination of water–rock interaction rates across different timescales.

Geothermal context

Upper Rhine Graben (URG)

The Upper Rhine Graben is part of the European Cenozoic Rift System that extends from the Mediterranean to the North Sea coast (Ziegler 1992). It is characterized by an NNE–SSW striking extension structure with a length of approximately 300 km and a width of up to ca. 40 km. The deep Hercynian basement consisting of Paleozoic granites is overlain by clastic sediments (sandstones) from Permian to Lower Triassic and by Middle Mesozoic to Cenozoic sediments. The base of the sediments in the center of the valley is ca. 3000 m deeper than at the valley shoulders (Ziegler 1992).

The Upper Rhine Graben offers favorable conditions for the exploitation of geothermal energy. This is supported by spatially varying local heat flow anomalies and temperature anomalies at large depths. Most of the thermal anomalies are related to large-scale fluid circulation (Pribnow and Schellschmidt 2000).

Bruchsal site (Germany)

The Bruchsal geothermal site is located at the eastern main boundary fault of the Upper Rhine Graben. The geothermal power plant consists of a borehole doublet: an injection well (GB1) and a production well (GB2) located at a distance of 1.5 km from each other. Because of the complex tectonic structure, the reservoir section at the injection well differs from that of the production well with respect to depth and thickness.

The geothermal reservoir is located in Permo-Triassic sedimentary rocks, characterized by large-scale normal faults of varying step heights, ranging between 20 and 350 m (Fig. 2). The hydrothermal reservoir is developed in a horizon comprising Middle Buntsandstein to Upper Rotliegend rocks (depth interval: 2220–2485 m). The main inflow zones are located in the fractured zones of the Upper Permian at the depth interval between 2440 and 2470 m (Joachim et al. 1987). Hydrothermal alteration processes resulted in an almost complete transformation of the original feldspars

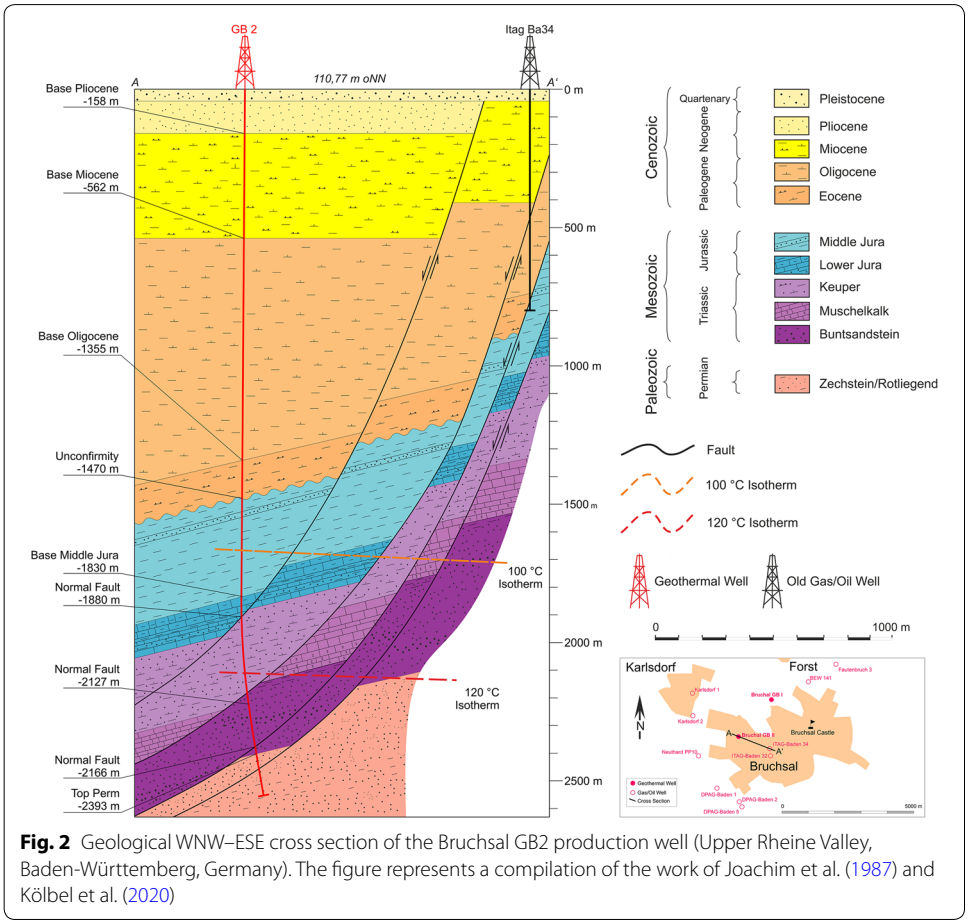

Fig. 2 Geological WNW–ESE cross section of the Bruchsal GB2 production well (Upper Rheine Valley, Baden-Württemberg, Germany). The figure represents a compilation of the work of Joachim et al. (1987) and Kölbel et al. (2020)

into clay minerals, and in large quantities of Fe-hydroxides as limonite coatings around quartz grains (Kölbel et al. 2020).

Borehole data of GB2 showed a bottom hole temperature of 134.7 °C at 2542 m depth, corresponding to a geothermal gradient of 55 K km^{-1}, and exceeding the typical average value for Central Europe of 30 K km^{-1}.

At present, the thermal water is produced with a flow rate of 24 L/s. Geochemical analysis of the NaCl brine showed high mineralization (TDS ≈ 130 g/l) including heavy metals and gases at a pH of 5 (Eggeling et al. 2013).

Activities of the primordial radionuclides ^{238}U, ^{232}Th and ^{235}U in the Upper Rotliegend amount to 18 Bq kg^{-1}, 17 Bq kg^{-1} and 0.8 Bq kg^{-1}, respectively. These are relatively low, but rather typical values for sandstones (Gascoyne 1992).

Methodology

Sampling and analytical methods

Brine samples were collected at a sampling point close to the GB2 well head at the Bruchsal geothermal site. Hydrogeochemical investigations were conducted on thermal water abstracted from the production well GB2 during fluid circulation. The sampling period spanned between October 2016 and May 2017. In total 32 water samples were collected. Major ions and selected trace elements were analyzed in the samples by ICP-OES, ion chromatography and photometry. Temperature, pH and conductivity were measured on-site. ^{238}U, ^{232}Th and ^{235}U decay series radionuclides (Fig. 1) were analyzed in 13 samples well GB2 to study their temporal variations in activities. The main research focus was on activity variations of radium isotopes (^{224}Ra, ^{223}Ra, ^{228}Ra, ^{226}Ra). Radium-sampling was conducted using gas-tight 1.2-l Marinelli beakers (type G-130 G) prepared with 2.5 ml 65% HNO_3 (suprapur) to inhibit precipitation of solids. Water samples were not filtered.

Gamma spectrometry surveys were carried out using a p-type HPGe coaxial detector of 30% efficiency (with respect to $3'' \times 3''$ NaI(Tl) detector). The germanium crystal had a diameter of 76 mm. The detector was embedded in a 10-cm lead shield to protect against background radiation. Specific activities of radium isotopes were determined by gamma spectrometry allowing simultaneous measurements without further sample preparation. The list of the gamma rays used for the determination of activities of radium isotopes is reported in Table 1. Measurements (M_{t1}) were performed immediately after sample collection to determine activities of the short-lived radium daughters (^{228}Ac, ^{212}Pb, ^{214}Pb). The measurement duration (Δt) was ca. 80,000 s (= 22.2 h). A second measurement (M_{t2}) was carried out after storing the sample for more than 42 h, but less than 350 h.

In addition, radionuclides of the ^{238}U, ^{232}Th and ^{235}U decay series were analyzed in an external certified laboratory. The activities of ^{238}U, ^{234}U, ^{230}Th, ^{226}Ra, ^{210}Po, ^{235}U, ^{227}Ac, ^{223}Ra, ^{232}Th, ^{228}Th and ^{224}Ra in the Bruchsal brine were measured by alpha spectrometry. ^{228}Ra was measured by beta counting. The accuracy of the gamma spectrometric method was checked by alpha spectrometry. Moreover, activities of uranium and thorium isotopes were determined which is not possible by gamma spectrometric measurements alone due to low U–Th activities in the brine samples.

Table 1 Nuclides employed for the determination of Ra activities in the Bruchsal brine

Nuclide of interest	Half-life	Measured nuclide	Eγ (keV)	Iγ (%)	Interfering nuclide	Eγ (keV)	Iγ (%)
^{226}Ra	1600 year	^{226}Ra	186.21	3.59			
		^{214}Pb	242.00	7.12			
			295.22	18.15			
			351.93	3.51	^{211}Bi	351.06	12.91
		^{214}Bi	609.31	44.60			
			1120.29	14.70			
			1764.49	15.10			
^{228}Ra	5.75 year	^{228}Ac	338.32	11.27	^{223}Ra	338.28	2.79
			911.07	25.80			
			968.90	15.80			
^{224}Ra	3.66 days	^{212}Pb	238.63	43.30			
		^{208}Tl	583.19	30.37			
^{223}Ra	11.0 days	^{223}Ra	154.30	5.62	^{228}Ac	153.98	0.72
			269.60	13.73	^{228}Ac	270.25	3.46
					^{219}Rn	271.23	10.8

Data of gamma ray energies (Eγ) and intensities (Iγ) are from Condomines et al. (2010)

Reflecting the sample point at well head, the radionuclide activities measured in the lab were corrected by considering the travel time of produced fluids from reservoir to surface (lag time correction) as well as the elapsed time since fluid sampling.

Brine density was calculated according to Mao and Duan (2008), considering reservoir temperature and pressure as well as the molality of the NaCl brine ($T = 135$ °C, $p = 250$ bar, M(NaCl) = 2.1 mol/kg). The resulting brine density is 1023.24 kg/m^3. The activities of dissolved radionuclides are reported as disintegration rate per fluid-mass (atoms s^{-1} kg^{-1}).

Calculation of Ra activities from gamma spectrometry

^{226}Ra

The ^{226}Ra activity was directly determined using its gamma ray energy at 186.2 keV. A possible interference with ^{235}U (185.7 keV) is negligible due to the low uranium activity shown by high-resolution ICP-MS. Alternatively, the gamma-peaks of ^{214}Pb and ^{214}Bi (daughters of ^{226}Ra and ^{222}Rn, respectively) can be used to calculate the ^{226}Ra activity. In this case, the measurement can be performed after 20 days at the earliest, because this time is required to reach secular radioactive equilibrium (assuming no radon loss).

^{223}Ra

154.3 keV gamma ray energy was used to determine the ^{223}Ra activity. Here the presence of an interfering peak from ^{228}Ac has to be considered (cf. Table 1). According to Condomines et al. (2010), ^{223}Ra activity based on the 154.3 keV peak can be corrected by:

$$\overline{\left(^{223}Ra\right)} = \frac{C}{C_S} \cdot \left[\left(^{223}Ra\right)_S + \left(^{228}Ac\right)_S \cdot \frac{\varepsilon_{Ac} I_{\gamma,\,Ac}}{\varepsilon_{Ra} I_{\gamma,\,Ra}} \right] - \overline{\left(^{228}Ac\right)} \cdot \frac{\varepsilon_{Ac} I_{\gamma,\,Ac}}{\varepsilon_{Ra} I_{\gamma,\,Ra}}, \tag{1}$$

where $\overline{\left(^{223}Ra\right)}$ and $\overline{\left(^{228}Ac\right)}$ are average activities integrated over the counting time. C and C_S are the counts for the sample and the standard, respectively. ε_{Ac} and ε_{Ra} are the

apparent efficiencies for ^{228}Ac and ^{223}Ra. $I_{\gamma,Ac}$ and $I_{\gamma,Ra}$ are gamma-ray intensities (cf. Table 1).

^{228}*Ra and* ^{224}*Ra*

^{228}Ra and ^{224}Ra are part of the decay scheme of the ^{232}Th decay series (cf. Fig. 1). Measurements of both Ra isotopes include the count rates of their short-lived daughters ^{228}Ac ($t_{1/2}$ = 6.13 h) and ^{212}Pb ($t_{1/2}$ = 10.64 h) which evolve through time during counting. The time-dependent evolution of the thorium decay series radionuclides is illustrated in Fig. 3 and can be described by a system of coupled differential equations. Their general solution was first given by Bateman (1910). A radioactive decay chain ($N_1 \rightarrow N_2 \rightarrow \ldots \rightarrow N_i$) with the decay constant λ_i can be described by the following differential equations:

$$\frac{dN_1}{dt} = -\lambda_1 N_1 \tag{2a}$$

$$\frac{dN_i}{dt} = \lambda_{i-1} N_{i-1} - \lambda_i N_i (i = 2, n) \tag{2b}$$

Assuming zero concentrations of all daughters at time zero,

$$N_1(0) \neq 0 \text{ and } N_i(0) = 0 \quad \text{when } i > 1 \tag{3}$$

Bateman (1910) expressed the concentration of nth radionuclide after time t as:

$$N_n(t) = \frac{N_1(0)}{\lambda_n} \sum_{i=1}^{n} \lambda_i \alpha_i exp[-\lambda_i t] \tag{4}$$

where the coefficients are calculated by

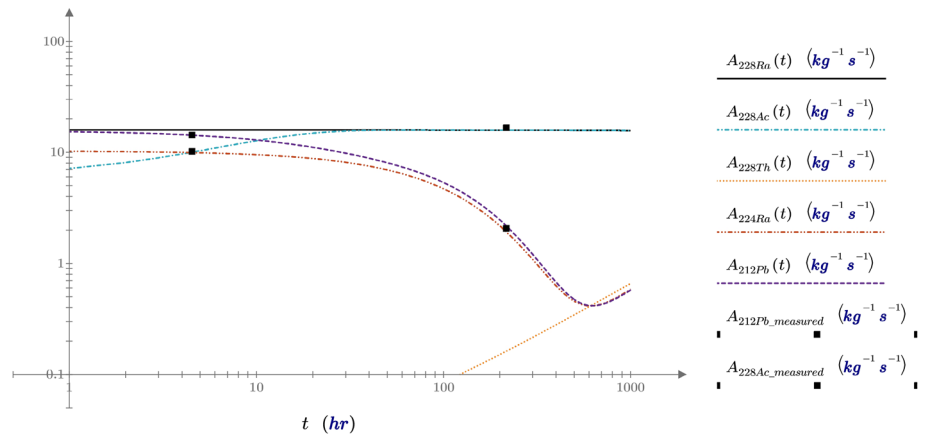

Fig. 3 Several successive transformations within the ^{232}Th decay series for the Bruchsal brine: The dotted lines represent the simulated time-dependent evolution over activities of ^{228}Ra and its daughters (^{228}Ra $\rightarrow$ ^{228}Ac $\rightarrow$ ^{228}Th $\rightarrow$ ^{224}Ra). Time after sampling (t) is found on the x-axis. Measured activities at the times of measuring t_1 and t_2 are plotted as dots. Calculations were performed by means of a CAS software (PTC Mathcad)

$$\alpha_i = \prod_{j=1}^{n} \frac{\lambda_j}{(\lambda_j - \lambda_i)} \quad (j \neq i) \tag{5}$$

Degering and Köhler (2011) adjusted Eq. (4) to the time-averaged activity expressed as:

$$\overline{A_i(t_d, \Delta t)} = \frac{1}{\Delta t} \int_{t_d}^{t_d+\Delta t} A_i(t)dt = \sum_{j=1}^{i} \alpha_{ij} \overline{\tau_j(t_d, \Delta t)} \tag{6}$$

where

$$\overline{\tau_j(t_d, \Delta t)} = \frac{1}{\Delta t \lambda_j} \tau_j(t_d)(1 - \tau_j(\Delta t) \tag{7}$$

$$\tau_j(t) = e^{-\lambda_j t} \tag{8}$$

The mathematical solution for the Bruchsal site was computed by employing Mathcad®. For better understanding, index notation of ^{228}Ra = A_1; ^{228}Ac = A_2, ^{228}Th = A_3 and ^{224}Ra = A_4 are used from here on.

The activity of ^{228}Ra at sampling time ($t = 0$) was determined from the ^{228}Ac activity after a waiting period t_d of minimum 42 h after sampling:

$$A_1(0) = \frac{A_2(t_d, \Delta t)}{\tau_1(t_d, \Delta t)} \tag{9}$$

^{224}Ra was determined by gamma-rays emitted by the daughter nuclides ^{212}Pb (238.6 keV) and ^{208}Tl (583.1 keV) with the ^{212}Pb/^{224}Ra ratio reaching a steady- state value of 1.14 after ca. 100 h:

$$A_4(0) = \frac{1}{\overline{\tau_4(t_d, \Delta t)}} \left(\overline{A_4(t_d, \Delta t)} - (c_1 A_1(0) + c_3 A_3(0)\right), \tag{10}$$

$$c_1 = \alpha_{41}\alpha_{31}\left(\overline{\tau_1(t_d, \Delta t)} - \overline{\tau_4(t_d, \Delta t)}\right) - \alpha_{43}\alpha_{31}\left(\overline{\tau_3(t_d, \Delta t)} - \overline{\tau_4(t_d, \Delta t)}\right), \tag{11}$$

$$c_3 = \alpha_{43}\left(\overline{\tau_3(t_d, \Delta t)} - \overline{\tau_4(t_d, \Delta t)}\right), \tag{12}$$

$$c_4 = \overline{\tau_4(t_d, \Delta t)}. \tag{13}$$

Results

Major and trace elements

Field parameter and major and minor element data are reported in Table 2. The Bruchsal brine is highly concentrated in chloride, sodium and other alkali metals and alkaline earth metals, containing up to 131 g/l of total dissolved solids (TDS). Furthermore, the brine is enriched in sulfate and hydrogen carbonate as well as heavy metals such as lead, arsenic, and cadmium. In contrast, the concentration of organic compounds is low. Eh–pH conditions are difficult to determine because of the change in pressure and

Table 2 Physical parameters and chemical composition of the Bruchsal geothermal fluid

	Flow rate [l/s]	$T_{sampling}$ [°C]	Conductivity at 25 °C [mS/cm]	pH []	Eh [mV]	TDS [g/l]
Mean	25.5	21.5	155.6	5.3	81	131
Min	23.3	18.7	152.5	5.0	91	127
Max	29.5	26.0	158.1	5.9	72	135
	K [mg/l]	**Na [mg/l]**	**Ca [mg/l]**	**Mg [mg/l]**	**Cl [mg/l]**	**SO_4 [mg/l]**
Mean	3523	40,543	9478	397	74,910	339
Min	3309	38,134	9052	361	73,250	299
Max	3642	42,765	9956	437	76,166	492
	Sr [mg/l]	**Ba [mg/l]**	**Br [mg/l]**	**HCO_3 [mg/l]**	**Fe [mg/l]**	**Fe^{2+} [mg/l]**
Mean	387	9.2	312	341	50.1	32.7
Min	362	6.7	284	255	49.2	26.3
Max	400	9.6	341	374	51.5	44.4
	Fe^{3+} [mg/l]	**Mn [mg/l]**	**Pb [mg/l]**	**As [mg/l]**	**Al [mg/l]**	**Cd [mg/l]**
Mean	19.4	25.7	3.0	9.7	1.8	0.2
Min	12.2	23.6	1.5	6.0	1.1	0.1
Max	24.0	27.5	5.5	12.0	2.6	0.4

Mean values are based on the analysis of 32 samples

temperature between reservoir and the sampling location at ground level. At the sampling point, pH values range between 5.0 and 5.9 [], while Eh values are relatively constant at ca. 81 mV (on average).

U–Th decay series radionuclides

Results of the investigated radionuclides are listed in Table 3. Relative uncertainties are quoted in percentage as two-standard deviations based on counting statistics. Generally, Ra (^{226}Ra, ^{228}Ra, ^{224}Ra, ^{223}Ra), Rn (^{222}Rn) and Pb (^{210}Pb, ^{212}Pb) are rather mobile in geothermal brine, while U (^{238}U, ^{234}U, ^{235}U), Th (^{232}Th, ^{228}Th, ^{230}Th), Po (^{210}Po) and Ac (^{227}Ac, ^{228}Ac) are less mobile, e.g., due to their adsorptive behavior or co-precipitation (Hammond et al. 1988). As a consequence, significant radioactive disequilibria form within the natural decay series (Fig. 4).

Activities of Th (^{230}Th, ^{232}Th and ^{228}Th) and U (^{238}U, ^{234}U, ^{235}U) isotopes in brine were below the limit of analytical determination. This suggests that in the reservoir uranium preferentially exists in the tetravalent state, forming insoluble phases such as UO_2 and $USiO_4$. Thorium is only stable in the tetravalent state; irrespective of the redox conditions, uranium requires a reducing environment to become tetravalent as in deep geothermal reservoirs (Attendorn and Bowen 1997).

In contrast, high levels of activity were observed for Ra isotopes (^{226}Ra, ^{228}Ra, ^{224}Ra, ^{223}Ra), ^{222}Rn and Pb isotopes (^{210}Pb, ^{212}Pb). Their activities are several orders of magnitude higher than those of their thorium progenitors. ^{222}Rn, is in slight excess relative to its parent ^{226}Ra.

Isotopes of Pb (^{210}Pb and ^{212}Pb) have high solubilities resulting in fluid activities > 15 Bq kg^{-1}. ^{210}Pb (A_{210Pb} = 25.8 Bq kg^{-1}) was found to be deficient relative to its progenitors ^{222}Rn (A_{222Rn} = 37.8 Bq kg^{-1}) and ^{226}Ra (A_{226Ra} = 29.0 Bq kg^{-1}), but still in

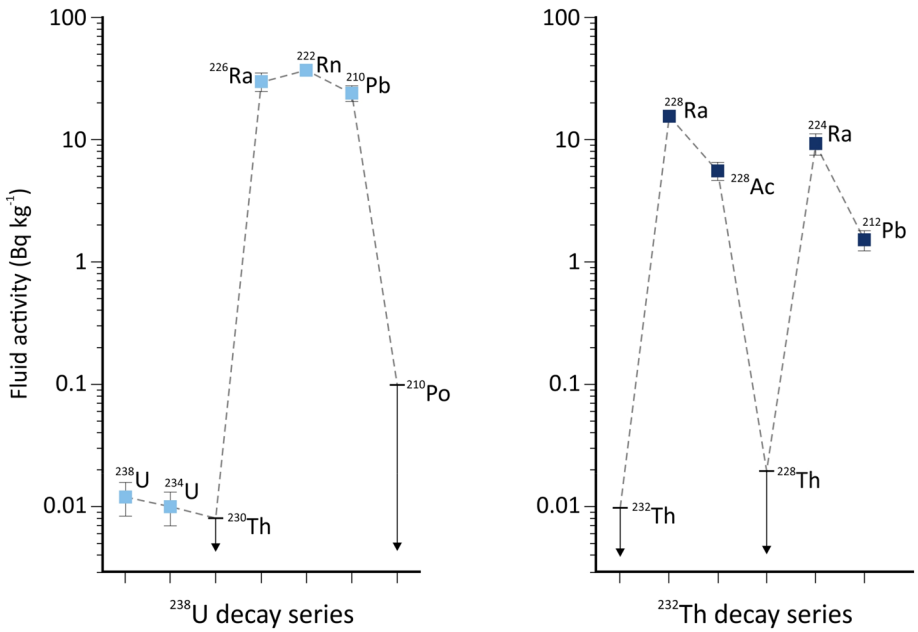

Fig. 4 Uranium and thorium series disequilibria: specific activity of ^{238}U and ^{232}Th and their decay products measured in the Bruchsal brine. Error bars represent uncertainties due to counting statistics ($\pm 2\,\sigma$). ^{230}Th, ^{210}Po, ^{233}Th and ^{228}Th activities are upper limits. Radionuclide movement down the decay chain is from left to right

Table 3 ^{238}U, ^{232}Th and ^{235}U decay series radionuclides in the Bruchsal brine samples

Decay series	Radionuclide	Specific activity (Bq kg^{-1})	Relative uncertainty (%)	Number of samples	Method
Uranium series	^{238}U	0.012	59	1	α-spectrometry
	^{234}U	0.01	66	1	α-spectrometry
	^{230}Th	< 0.08		1	α-spectrometry
	^{226}Ra	29.0	8.3	13	γ-spectrometry
	^{222}Rn	37.8	7.4	1	γ-spectrometry
	^{210}Pb	25.8	26	12	γ-spectrometry
	^{210}Po	< 0.1		1	α-spectrometry
Actinium series	^{235}U	< 0.004		1	α-spectrometry
	^{227}Ac	< 0.1		1	α-spectrometry
	^{223}Ra	0.47	60	13	γ- spectrometry
Thorium series	^{232}Th	< 0.01		1	α-spectrometry
	^{228}Ra	15.9	5.8	13	γ-spectrometry
	^{228}Ac	6.1	27	2	γ-spectrometry
	^{228}Th	< 0.02		1	α-spectrometry
	^{224}Ra	10.3	7.5	13	γ-spectrometry
	^{212}Pb	15.7	6.4	2	γ-spectrometry

Relative uncertainties are quoted in percentage ($\pm 2\sigma$ from counting statistics)

the same order of magnitude indicating that Ra, Rn and Pb have a comparable mobility in the Bruchsal geothermal system.

The activity of ^{210}Po is below the limit of determination. The low ^{210}Po activity in comparison to its parent ^{210}Pb suggests removal of ^{210}Po from the brine. The same applies to isotopes of actinium: the short-lived ^{228}Ac (A_{228Ac} = 6.1 Bq kg^{-1}) of the thorium decay series is deficient relative to its parent ^{228}Ra (A_{228Ra} = 15.9 Bq kg^{-1}). ^{227}Ac, an isotope of the ^{235}U decay series, was found to have a lower activity than its daughter ^{223}Ra indicating the rapid depletion of ^{227}Ac from brine.

The rock/brine activity ratio (R_c) is a measure of the relative mobility of the isotopes (Zukin et al. 1987). Values for R_c were determined based on analyses of brine (Table 3) and rock samples from borehole cuttings (Kölbel et al. 2020). The results are summarized in Table 4. High R_c values in the order of magnitude of 10^2 for isotopes of U (^{238}U, ^{234}U, ^{235}U) and Th (^{232}Th, ^{228}Th, ^{230}Th) reflect the affinity of the nuclides to the surface of the solids for both elements. In turn, isotopes of Ra (^{226}Ra, ^{228}Ra, ^{224}Ra, ^{223}Ra) and Pb (^{210}Pb and ^{212}Pb) have lower R_c values and therefore, a relatively high mobility in the investigated geothermal system is implied.

^{228}Th (a decay product of ^{232}Th) has a rather low R_c value compared to ^{232}Th. This reflects a better accessibility of ^{228}Th to the geothermal brine because of the good solubility of its ^{228}Ra progenitor. Following the decay of ^{228}Ra, ^{228}Th is adsorbed onto grain surfaces producing a comparatively high activity compared to the activity of the ^{232}Th isotope.

In summary, isotopes of thorium, polonium and actinium generally display low levels of activity in the brine as a result of their poor solubility. The processes of removal of the above isotopes from solution are most likely adsorption and/or co-precipitation.

Radium isotopes

Radium isotopes (^{226}Ra, ^{228}Ra, ^{224}Ra, ^{223}Ra) were measured several times during power plant operation. Radium activities as well as activity ratios of Ra isotopes (^{228}Ra/^{226}Ra, ^{224}Ra/^{228}Ra, ^{223}Ra/^{226}Ra) are listed in Table 5.

Table 4 R_c values of Th–U decay series radionuclides

Isotope	Rock activity (Bq kg^{-1})	R_c values	Half-life
^{238}U	18.0	1.5×10^3	4.47×10^9 y
^{235}U	0.8	$> 2.1 \times 10^2$	7.04×10^8 y
^{234}U	19.0	1.9×10^3	2.46×10^5 y
^{232}Th	17.0	$> 1.7 \times 10^3$	1.41×10^{10} y
^{230}Th	19.0	$> 2.4 \times 10^2$	7.54×10^4 y
^{228}Th	19.0	$> 9.5 \times 10^2$	1.91 years
^{226}Ra	43.0	1.5	1600 years
^{228}Ra	17.0	1.1	5.75 years
^{223}Ra	0.8	1.8	11.43 days
^{224}Ra	19.0	1.7	3.66 days
^{210}Pb	37.0	1.4	22.30 years
^{212}Pb	19.0	1.2	10.64 h

R_c is defined as the ratio of rock activity relative to average fluid activity (cf. Table 3)

Table 5 Radium activities and activity ratios in brine collected from GB2 well (measurement campaign 2016/2017)

Sample no.	Sampling date	^{226}Ra	^{228}Ra	^{224}Ra	^{223}Ra	^{228}Ra/^{226}Ra	^{224}Ra/^{228}Ra	^{223}Ra/^{226}Ra
GB2-p1z1-001	13.10.2016	28.8 ± 2.4	15.2 ± 0.8	10.6 ± 0.6	0.41 ± 0.25	0.53 ± 0.07	0.70 ± 0.08	0.01 ± 0.01
GB2-p1z1-002	18.10.2016	27.6 ± 2.6	14.9 ± 0.8	10.0 ± 0.4	0.37 ± 0.22	0.54 ± 0.08	0.67 ± 0.06	0.01 ± 0.01
GB2-p1z1-003	24.10.2016	28.1 ± 2.4	15.5 ± 0.8	10.4 ± 0.4	0.48 ± 0.29	0.55 ± 0.08	0.67 ± 0.06	0.02 ± 0.01
GB2-p1z1-004	28.10.2016	29.3 ± 2.8	16.4 ± 0.9	11.5 ± 0.6	0.53 ± 0.32	0.56 ± 0.08	0.70 ± 0.08	0.02 ± 0.01
GB2-p1z1-005	04.11.2016	27.2 ± 2.2	16.1 ± 0.8	9.0 ± 2.0	0.74 ± 0.44	0.59 ± 0.08	0.56 ± .15	0.03 ± 0.02
GB2-p1z1-006	16.11.2016	28.0 ± 2.4	15.3 ± 0.8	10.4 ± 0.6	0.51 ± 0.31	0.55 ± 0.08	0.68 ± 0.07	0.02 ± 0.01
GB2-p1z1-007	17.01.2017	29.5 ± 2.4	15.5 ± 0.8	10.1 ± 0.8	0.61 ± 0.37	0.53 ± 0.07	0.65 ± 0.09	0.02 ± 0.01
GB2-p1z1-008	04.04.2017	30.3 ± 2.2	16.0 ± 0.7	10.3 ± 0.4	0.32 ± 0.19	0.53 ± 0.06	0.64 ± 0.05	0.01 ± 0.01
GB2-p1z1-009	11.04.2017	32.0 ± 2.4	16.7 ± 0.9	9.7 ± 1.0	0.36 ± 0.22	0.52 ± 0.07	0.58 ± 0.09	0.01 ± 0.01
GB2-p1z1-010	27.04.2017	29.9 ± 2.4	16.0 ± 0.8	10.6 ± 0.6	0.44 ± 0.26	0.54 ± 0.07	0.66 ± 0.07	0.02 ± 0.01
GB2-p1z1-011	02.05.2017	27.8 ± 2.4	16.4 ± 0.8	10.7 ± 0.4	0.50 ± 0.30	0.59 ± 0.08	0.65 ± 0.06	0.02 ± 0.01
GB2-p1z1-012	08.05.2017	28.9 ± 2.4	16.2 ± 0.8	11.1 ± 0.4	0.43 ± 0.26	0.56 ± 0.07	0.69 ± 0.06	0.02 ± 0.01
GB2-p1z1-013	15.05.2017	30.0 ± 2.4	16.1 ± 0.8	10.1 ± 0.4	0.45 ± 0.27	0.54 ± 0.07	0.63 ± 0.06	0.02 ± 0.01

Measured values are reported in Bq kg^{-1}. The quoted errors are 2σ-deviations derived from counting statistics

The highest activities range from 27 to 32 Bq kg^{-1} and are identified for the long-lived ^{226}Ra isotope. ^{228}Ra, ^{224}Ra and ^{223}Ra activities show lower values that vary between 15 and 17 Bq kg^{-1}, 9 and 12 Bq kg^{-1}, and 0.3 and 0.7 Bq kg^{-1}, respectively. Variation in activity levels of the radium isotopes are likely a consequence of analytical uncertainties and steady state in activities of the radium isotopes can be assumed.

This observation is also made with the activity ratios of radium that are principally constant within 2σ analytical uncertainties during the period of sampling: ^{228}Ra/^{226}Ra, ^{224}Ra/^{228}Ra and ^{223}Ra/^{226}Ra ratios display mean values of 0.55 ± 0.07, 0.65 ± 0.07 and 0.02 ± 0.01.

Gamma spectrometry results from earlier analysis (cf. Table 6), however, indicate that Ra activity in brine has increased over the past years. This particularly applies to ^{226}Ra and ^{228}Ra whose activities both increased by 25% resulting in a constant ^{228}Ra/^{226}Ra ratio (0.53 ± 0.09 in 1986 and 0.55 ± 0.07 in 2016/17). However, the short-lived ^{224}Ra activity has been more or less stable since 1986 resulting in a decrease in the ^{224}Ra/^{228}Ra activity ratio over the past 30 years from 0.75 in 1986 to 0.65 in 2016.

Modelling the disequilibria in water–rock systems

Water–rock interaction processes in the Bruchsal geothermal reservoir were mathematically modeled based on Ku et al. (1992). This model allows for physico-chemical reactions as well as advective transport. The model is robust in terms of input parameters

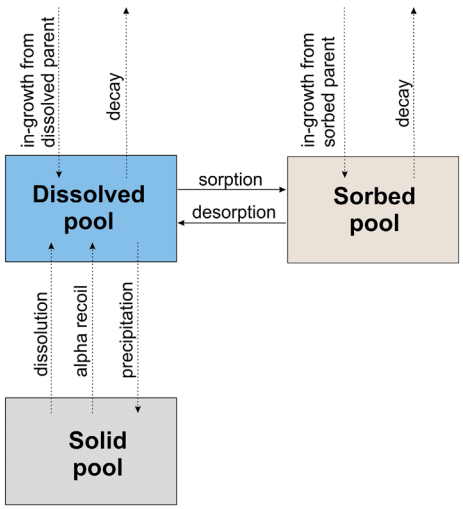

Fig. 5 Schematic representation of the water–rock interaction model suggested by Ku et al. (1992). Reversible and irreversible processes are indicated by arrows with solid and dashed lines. The figure was designed based on Ku et al. (1998)

Table 6 Radium activities (Bq kg^{-1}) and their ratios measured in August 1986 from a brine sample collected from GB2 production well

Ra isotopes	Activity in brine
^{224}Ra	9.1 ± 1.6
^{228}Ra	12.1 ± 1.1
^{226}Ra	22.9 ± 1.8
Isotopic ratio	**Activity in brine**
^{224}Ra/^{228}Ra	0.75 ± 0.20
^{228}Ra/^{226}Ra	0.53 ± 0.09

Reported errors are 2σ uncertainties. Data are provided by EnBW and corrected for the site-specific fluid density of $\rho_b = 1023.24$ kg/m^3

and focuses on the simulation of the behavior of radium in the rock–brine environment. Employment of the various radium isotopes provides a way of quantifying relevant parameters of the water–rock system due to their wide range of half-lives. Theoretically, the model can be applied to all elements with numerous instable isotopes such as U (^{238}U, ^{235}U, ^{234}U) and Th (^{234}Th, ^{232}Th, ^{231}Th, ^{230}Th, ^{228}Th, ^{227}Th). However, Th–U isotopes are not used in this study due to their poor solubility in the Bruchsal brine and the resulting lack of data.

Model assumptions suggested by Ku et al. (1992)

The processes of sorption–desorption and dissolution–precipitation of radionuclides are determined by reaction kinetics. Ku et al. (1992) subdivided three "pools" in which radionuclides can reside: the dissolved, adsorbed and solid pool. Figure 5 depicts a schematic representation of the conceptual model including water–rock interaction

processes and the three different "pools". Model parameters are listed in Table 7. Ku et al. (1992) defined the following model assumptions:

(1) In the dissolved "pool", radionuclides are exchangeable with those in the adsorbed pool, but not with those in the solid "pool".
(2) Transfer of radionuclides between the dissolved and solid "pools" is achieved in particular by dissolution, co-precipitation and alpha-recoil.
(3) Dissolution and precipitation are considered irreversible because dissolved nuclides have limited and very slow communication with the solid "pool" which is located further inside the rock matrix.
(4) Alpha-recoil input from the adsorbed and dissolved "pools" to the solid "pool" is negligible.
(5) Distributions of radionuclides in solid, adsorbed, and dissolved "pools" remain stationary.

Governing equations

Based on mass balance, the activity of a given radionuclide dissolved in a volume of brine with a constant density can be expressed as (Luo et al. 2000):

$$Q + P_r + P_w + R_f' A' = k_p C + R_f A, \tag{14}$$

where Q is the supply rate by water flow, atoms kg^{-1} s^{-1}; P_w is the supply rate of radionuclide to fluid by dissolution, atoms kg^{-1} s^{-1}; P_r is the supply rate of radionuclide to fluid by alpha-recoil, atoms kg^{-1} s^{-1}; R_f is the retardation factor due to adsorption and desorption, dimensionless; A is the radionuclide activity in brine, atoms kg^{-1} s^{-1} ($= \lambda C$); k_p is the first-order precipitation rate constant, s^{-1}; C is the radionuclide concentration in brine, atoms kg^{-1}; and $'$ is the superscript referring to the radioactive parent.

The retardation factor R_f is formulated as follows (Krishnaswami et al. 1982):

$$R_f = 1 + K = 1 + \frac{k_1}{k_2 + \lambda}, \tag{15}$$

where λ is the radioactive decay constant of radionuclide, s^{-1}; K is the dimensionless distribution coefficient; k_1 is the first-order adsorption rate constant, s^{-1}; and k_2 is the first-order desorption rate constant, s^{-1}.

For all radium isotopes whose thorium parents are quite insoluble in the geothermal fluid, $R_f' A'$ is negligible:

$$Q + P_r + P_w = k_p C + R_f A. \tag{16}$$

Furthermore, processes of dissolution and precipitation will not influence the activity of short-lived radionuclides and thus, by setting $P_W = 0$ and $k_p C = 0$, Eq. (16) may be simplified to

$$Q + P_r = R_f A, \tag{17}$$

where

$$Q = \frac{(C^i - C)}{\tau_b}. \tag{18}$$

C^i and C are initial and measured concentrations, respectively, and τ_b is the transit time of brine in the aquifer. Positive or negative values of Q denote net gain or loss due to fluid flow, i.e., advective transport (Luo et al. 2000).

Alpha-recoil

Alpha-recoil describes a process in which a radioactive daughter is mobilized from its initial position by the energy of an alpha decay (Sun and Semkow 1998). During the decay, an atomic nucleus emits an alpha particle. The released ionizing radiation has an energy content of 4–6 MeV. Because of the law of conservation of momentum, the emitted alpha particle and recoiling nucleus will each have a well-defined energy after the decay. Because of its smaller mass, most of the kinetic energy is transferred to the alpha particle. The recoiling nucleus will have a kinetic energy in the order of 100 keV (Sun and Semkow 1998). Nevertheless, the energy transfer to the decay product is high enough to shift atoms that are close to the mineral surface out of the mineral grain into the pore space (Fig. 6). The probability of recoiling out of mineral grains depends on the isotope recoil distance and the number of previous alpha decays. While ^{228}Ra is directly formed by the decay of ^{228}Th, ^{226}Ra is formed by three alpha decays of ^{238}U. Thus, the probability of ^{226}Ra to end up in the fluid by alpha-recoil is significantly greater than the probability for ^{228}Ra due to the greater amount of the three alpha energies.

Alpha-recoil supply rates (P_r) for radium isotopes can be estimated from the activities of the decay series progenitors (^{238}U, ^{235}U and ^{232}Th) in the adjoining rock expressed as (e.g., Kigoshi 1971):

$$P_r = \overline{A'}\varepsilon_i r S \rho_s, \tag{19}$$

where $\overline{A'}$ is the parent activity in solids (atoms kg^{-1} s^{-1}), r is the recoil distance (Å), ε_i is the recoil efficiency for nuclide i (), S is the surface area of solids, expressed as area of solid per volume of fluid contacting the solids (m^2 m^{-3}) also called flow-wetted surface and ρ_s is the density of solid (kg m^{-3}).

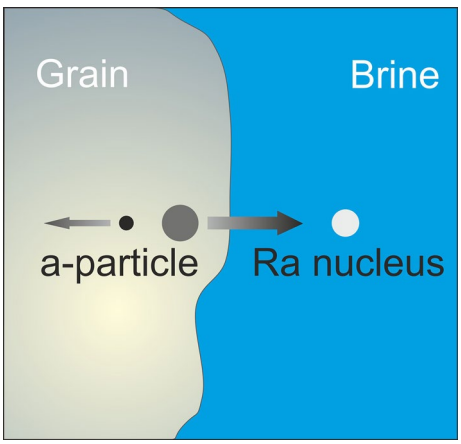

Fig. 6 Schematic diagram of alpha-recoil mechanism. Mobilization of a radioactive daughter from its initial position by the energy of an alpha decay. Arrow size reflects energy content

Table 7 Parameters used in the water–rock interaction model (Ku et al. 1992)

Symbol	Parameter	SI units
A	Specific activity of a dissolved radionuclide	Bq kg^{-1}
A^*	Specific activity of a dissolved radionuclide originated from diffusional flux	Bq kg^{-1}
A_a	Specific activity of an adsorbed radionuclide	Bq kg^{-1}
$\overline{A}$	Specific activity of a radionuclide in solids	Bq kg^{-1}
C	Concentration of a dissolved radionuclide	atoms kg^{-1}
C^i	Initial concentration of a dissolved radionuclide	atoms kg^{-1}
D_m	Diffusion coefficient of a radionuclide	m^2 s^{-1}
F	Diffusional flux of a nuclide into larger fractures	Bq m^{-2}
e_{Ra}	Radium recoil efficiency relative to ^{222}Rn	–
ε_i	Recoil efficiency for nuclide i	–
ϕ	Porosity of the aquifer	–
k_1	First-order adsorption rate constant	s^{-1}
k_2	First-order desorption rate constant	s^{-1}
k_p	First-order precipitation rate constant	s^{-1}
k_w	First-order dissolution rate constant	s^{-1}
K	Dimensionless distribution coefficient	–
K_d	Distribution coefficient	L kg^{-1}
λ	Radioactive decay constant of radionuclide	s^{-1}
M_b	Mass of brine	kg m^{-3}
M_r	Mass of rock	kg m^{-3}
P	Supply rate of radionuclide to brine	Bq kg^{-1}
P_d	Supply rate of radionuclide to brine by desorption	Bq kg^{-1}
P_r	Supply rate of radionuclide to brine by alpha-recoil	Bq kg^{-1}
P_r^*	Supply rate of radionuclide to brine by alpha-recoil in consideration of diffusional flux	Bq kg^{-1}
P_w	Supply rate of radionuclide to brine by dissolution process	Bq kg^{-1}
Q	Supply rate of radionuclide by water flow	Bq kg^{-1}
r	Recoil distance	m
R_f	Retardation factor due to adsorption and desorption	–
R_f^*	Retardation factor due to precipitation as well as adsorption and desorption	–
ρ_b	Fluid density	kg m^{-3}
ρ_s	Density of aquifer solid	kg m^{-3}
S	Surface area of solids, expressed as area of solid per volume of fluid contacting the solids	m^2 m^{-3}
S_a	Scavenging rate of radionuclide from brine by adsorption to rock surfaces	Bq kg^{-1}
S_p	Scavenging rate of radionuclide from brine by co-precipitation with minerals	Bq kg^{-1}
τ_b	Transit time of brine in the aquifer	s
$\tau_{p,i}$	Mean time for nuclide i in solution to precipitate in minerals	s
$\tau_{w,i}$	Mean time for leach nuclide i from solid phases	s
w_f	Fracture width	m
v_f	Advection velocity of fracture fluid	m s^{-1}
x	Distance	m
	Superscript referring to radioactive parent	–

For the geothermal site in Bruchsal, the average progenitor activities ($\overline{A'}$) in the reservoir section are ^{238}U = 18.0 Bq kg^{-1}, ^{232}Th = 17.0 Bq kg^{-1} and ^{235}U = 0.8 Bq kg^{-1} (Kölbel et al. 2020). Surface area per mass is about 2000 m^2 kg^{-1} for the Permo-Triassic sandstones (Heap et al. 2019). This corresponds to a flow-wetted surface of 1.0×10^8 m^2 m^{-3} based on a porosity of 0.05. Sun and Semkow (1998) published data of Ra recoil distances

Table 8 Average and maximum recoil distances of radium isotopes in quartz which is chosen as the host due to the mineralogical composition of the aquifer

Decay	Average distance (Å)	Maximum distance (Å)
$^{230}Th \rightarrow {}^{226}Ra$	370.3	663.2
$^{232}Th \rightarrow {}^{228}Ra$	331.3	609.8
$^{228}Th \rightarrow {}^{224}Ra$	406.6	763.3

Data originate from Sun and Semkow (1998)

of 800 Å in the surface zone of quartz obtained from Monte Carlo simulations (Table 8). Since recoil efficiencies for radium isotopes are not that easy to determine, ε_i is part of the discussion.

Retardation factor and distribution coefficient

The retardation factor R_f describes the flow rate of the fluid relative to the rate of migration of a radionuclide in the flow (Ku et al. 1992). The separation between the adsorbed and dissolved nuclides through chemical exchanges might be stated by the dimensionless distribution coefficient K (Krishnaswami et al. 1982):

$$K = \frac{A_a}{A}, \tag{20}$$

where A_a is the activity of an adsorbed radionuclide (atoms per equivalent fluid-volume) and A is the radionuclide activity dissolved in solution (atoms per fluid-volume).

Since distribution coefficients are usually determined by adsorption–desorption experiments in the laboratory and therefore, expressed in units of volume per mass, K can be derived from

$$K = K_d \left[\frac{\rho_s (1 - \phi)}{\phi} \right], \tag{21}$$

where K_d is the distribution coefficient, volume mass^{-1}; ρ_s is the density of aquifer solids, mass solid volume^{-1}; and ϕ is the porosity of the aquifer, dimensionless.

Krishnaswami et al. (1982) expressed R_f and K in terms of adsorption and desorption rate constants, k_1 and k_2:

$$R_f = 1 + K = \frac{k_1 + k_2 + \lambda}{k_2 + \lambda} = \frac{1}{\Omega}, \tag{22}$$

$$k_1 = \frac{\left(\lambda_i - \lambda_j\right)(1 - \Omega_i)\left(1 - \Omega_j\right)}{\left(\Omega_i - \Omega_j\right)}, \tag{23a}$$

$$k_2 = \frac{\Omega_i \Omega_j \left(\lambda_j - \lambda_i\right) + \lambda_i \Omega_j - \lambda_j \Omega_i}{\left(\Omega_i - \Omega_j\right)}, \tag{23b}$$

where i and j refer to two isotopes of the same element and Ω is the ratio of the activity of a nuclide in solution, λC, to its rate of production P:

$$\Omega = \frac{\lambda \mathrm{C}}{\mathrm{P}}. \tag{24}$$

Since these authors did not consider dissolution processes, the supply rate P only includes recoil (P_r) and in situ production (λ'C') and thus, this model is only valid for radionuclides with half-lives less than 10 years (Appendix 1, Krishnaswami et al. 1982).

Precipitation and dissolution

The role of precipitation and dissolution processes becomes more apparent for longer-lived radionuclides. Rate constants for precipitation and dissolution may be calculated by the mass balances of radium isotopes.

Hammond et al. (1988) defined radium input to brine by dissolution processes, P_w (atoms s^{-1} kg^{-1}), by the following equation:

$$P_w = \frac{k_w \overline{A}}{\lambda}, \tag{25}$$

where $\overline{A}$ is the radium activity in rocks (atoms kg^{-1} s^{-1}), k_w is the first-order rate constant for dissolution (s^{-1}), and λ is the decay constant of the respective radium isotope (s^{-1}).

The converse process, radium co-precipitation with minerals, S_p (atoms s^{-1} kg^{-1}), can be expressed by

$$S_p = k_p C, \tag{26}$$

where k_p is the first-order rate constant for precipitation (s^{-1}) and C the concentration in brine (atoms kg^{-1}).

Model performance

The introduced mass balance approach was modeled using Mathcad®, a numerical software with computer algebra system (CAS) capabilities. In order to check the CAS approach, MIN3P, a multicomponent reactive transport code, was employed (Mayer et al. 2002).

MIN3P is a general-purpose flow and reactive transport code for variably saturated media providing a high degree of flexibility with respect to the definition of the reaction network. Advective–diffusive transport in the water phase and diffusive transport in the gas phase are included. Equilibrium reactions considered are aqueous complexation, gas partitioning between phases, oxidation–reduction, ion exchange, and surface complexation. The reaction network is designed to handle kinetically controlled intra-aqueous and dissolution–precipitation reactions. All reactions can be defined through databases of MINTEQA2 (Allison et al. 1991) and PHREEQC2 (Parkhurst and Appelo 1999).

Table 9 lists the set of data that were used for the comparison. Input parameters correspond to the physical parameters of the Bruchsal site which are required for reactive transport modelling (Joachim et al. 1987).

Recoil mechanism

Since MIN3P treats the recoil mechanism as an intra-aqueous reaction, recoil supply rates were specified in the respective database file. Assuming that short-lived nuclides are mainly controlled by alpha-recoil, ^{224}Ra was used as an example to test the accuracy of the recoil term. Figure 7 illustrates the results of the comparison between MIN3P and Mathcad®.

Kinetic approach for solid solutions

Co-precipitation of radium with barite is an important process affecting radionuclide reactive transport in rock formations. It is generally described using a solid solution model (Parkhurst and Appelo 2013). Commonly, geochemical equilibria are quantified by the law of mass action. A suitable example is given by the reaction of two components A and B with their stoichiometric constants a and b. Considering A and B as the aqueous components and AB as the solid-phase components ($aA + bB \rightleftharpoons AB$) leads to the equilibrium constant

$$K_{eq} = \frac{\{A\}^a \{B\}^b}{\{AB\}}, \tag{27}$$

where brackets {} represent the activity of the components. For the condition of a homogeneous solid, its activity is assumed unity, hence Eq. (27) is simplified to $K_{eq} = \{A\}^a \{B\}^b$, generally known as the solubility product of AB.

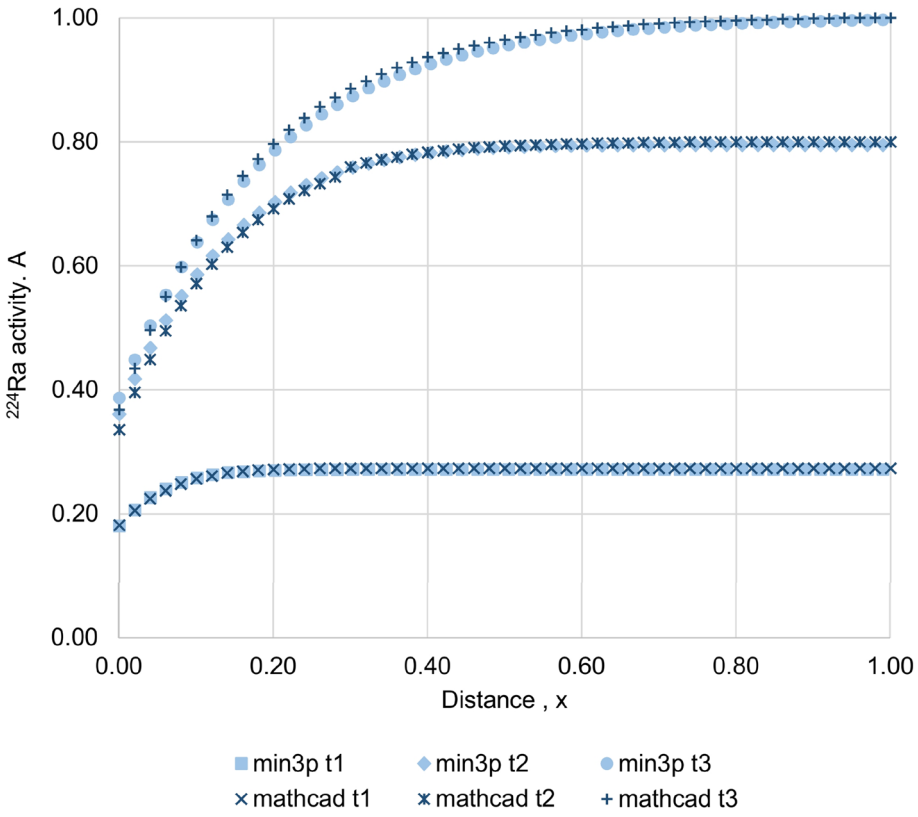

Fig. 7 Comparison of MIN3P and CAS model for one-dimensional transport of ^{224}Ra along a flow line, calculated at different half-lives ($t_1 = 0.5\ t_{1/2}$; $t_2 = 2\ t_{1/2}$; $t_3 = 45\ t_{1/2}$)

For a solid solution, i.e., a mixture of several constituents, this simplification does not hold. The specific solid-phase activity becomes dependent on its mole fraction X_i, yielding a set of concurrent equations. For simplicity, we neglect a potential non-ideality within the solid mixture, which would require the introduction of non-unity activity coefficients. It might as well be noted that often K_{eq} is defined in a reciprocal way. In the given background the two reactions are

$$Ba^{2+}SO_4^{2-} \rightleftharpoons BaSO_4 \tag{28a}$$

$$Ra^{2+}SO_4^{2-} \rightleftharpoons RaSO_4 \tag{28b}$$

with the associated solubility products

$$K_{Ba} = \frac{\left\{Ba^{2+}\right\}\left\{SO_4^{2-}\right\}}{X_{BaSO4}}, \tag{29a}$$

$$K_{Ra} = \frac{\left\{Ra^{2+}\right\}\left\{SO_4^{2-}\right\}}{X_{RaSO4}}. \tag{29b}$$

The equilibrated solution to this set of equations is a bit more cumbersome to achieve and the reader may be referred to, e.g., Rodriguez-Galan and Prieto (2018). However, if the equilibrium can be approached in a kinetic simulation, the forward and backward reactions can be separated and make use of Lasaga's principle of detailed balancing (Lasaga 1998) to obtain a considerably more straightforward procedure:

$$Ba^{2+}SO_4^{2-} \rightarrow BaSO_4 \tag{30a}$$

$$BaSO_4 \rightarrow Ba^{2+}SO_4^{2-} \tag{30b}$$

and

$$Ra^{2+}SO_4^{2-} \rightarrow RaSO_4 \tag{31a}$$

$$RaSO_4 \rightarrow Ra^{2+}SO_4^{2-} \tag{31b}$$

with the kinetic rate expressions

$$R_+ = k_+\left\{Ba^{2+}\right\}\left\{SO_4^{2-}\right\}, \tag{32a}$$

$$R_- = k_- X_{BaSO4}, \tag{32b}$$

in terms of the total reaction

$$R_t = k_+\left\{Ba^{2+}\right\}\left\{SO_4^{2-}\right\} - k_- X_{BaSO4} = k_+\left\{Ba^{2+}\right\}\left\{SO_4^{2-}\right\}\left(1 - \frac{IAP}{K_{eq}}\right). \tag{33}$$

Resulting in the forward activity product time an affinity term (1-IAP/K_{eq}), of which IAP is the complete ion activity product at current condition $X_{BaSO4}/(\{Ba^{2+}\}\{SO_4{}^{2-}\})$, and K_{eq} is its counterpart for equilibrium conditions.

Assuming that radium is always present in concentrations orders of magnitude lower compared to barium, so that the solid fraction only remains relevant for Ra^{2+}, it follows

$$X_{BaSO4} = \frac{\{BaSO_4\}}{\{RaSO_4\} + \{BaSO_4\}} \cong 1 \quad as\{Ba\} \gg \{Ra\}, \tag{34a}$$

$$X_{RaSO4} = \frac{\{RaSO_4\}}{\{RaSO_4\} + \{BaSO_4\}} \cong \frac{\{RaSO_4\}}{\{BaSO_4\}}. \tag{34b}$$

That allows treating barite dissolution/precipitation as a kinetic reversible process as given in the database, independent of the radium co-precipitation process, leaving the two kinetic rate expressions ($k1+$ and $k1-$) for radium left to solve for separately, with lumped rate constants k_+/k_-:

$$R_+ = \frac{k_+}{k_-}\left\{Ba^{2+}\right\}\left\{SO_4^{2-}\right\}, \tag{35a}$$

$$R_- = X_{RaSO4}. \tag{35b}$$

MIN3P's solid solution term was checked based on literature data (Grandia et al. 2008) resulting in (Ra,Ba)SO_4 equilibrium lines which have a similar slope for varying natural Ra–Ba trends (Fig. 8). The equilibrium line for the Bruchsal site shows the same trend as model-derived equilibrium lines from Grandia et al. (2008). Start and end point of the solid line is defined by the fluid-specific barium concentration and ^{226}Ra activity in brine.

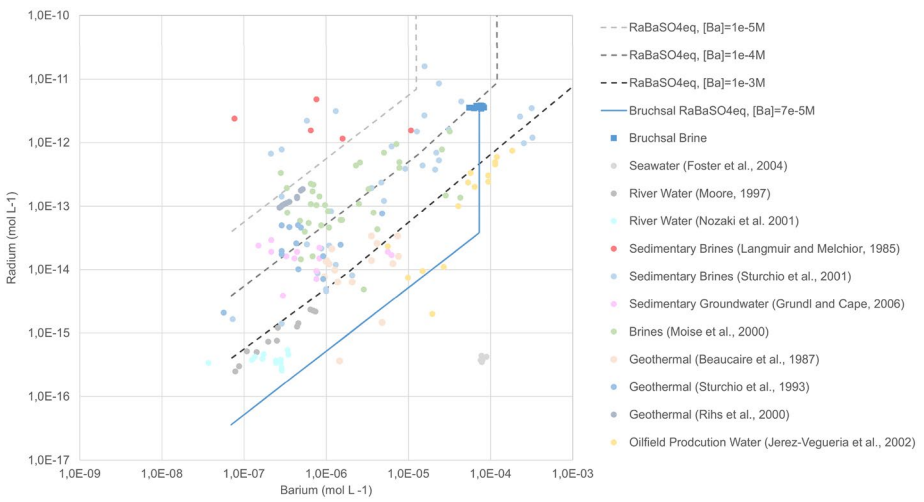

Fig. 8 Re-calculation of radium co-precipitation with barite from literature data (Grandia et al. 2008). Calculations result in (Ra,Ba)SO_4 equilibrium lines having a similar slope for varying natural Ra–Ba trends

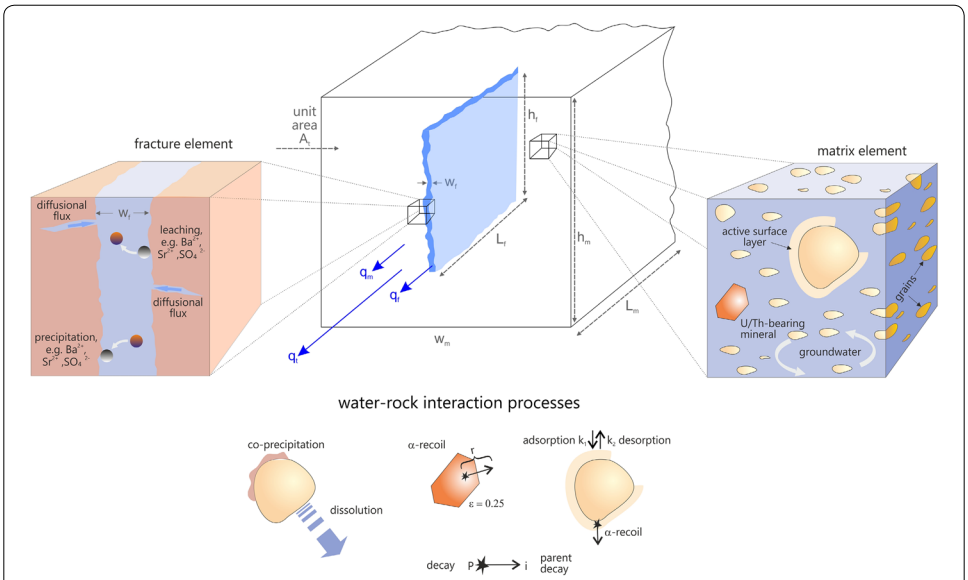

Fig. 9 Conceptual model for the Bruchsal geothermal site: Fracture-dominated radionuclide transport within the reservoir section in consideration of the physico-chemical water–rock interactions (adsorption–desorption, dissolution–precipitation, alpha-recoil) which take place to varying extent in both, the fracture and matrix element (figure extended after Tricca et al. 2000)

Table 9 Site-specific input parameter used for the model comparison between Mathcad® and MIN3P

Parameter	Symbol	Unit	Value
Porosity	ϕ	–	0.05
Hydraulic conductivity	k_f	m s^{-1}	4.3×10^{-6}
Darcy velocity	v_f	m s^{-1}	3.2×10^{-8}
Longitudinal dispersion	α_L	m	0.1

Data from Joachim et al. (1987)

Table 10 Recoil efficiency for radium (e_{Ra}) relative to ^{222}Rn (data originate from Krishnaswami et al. 1982) as well as model-derived rates of alpha-recoil supply (P_r) for the geothermal system in Bruchsal

Decay	e_{Ra} ()	P_r (atoms kg^{-1} s^{-1})
$^{230}Th \rightarrow {}^{226}Ra$	0.961	40
$^{232}Th \rightarrow {}^{228}Ra$	0.769	25
$^{227}Th \rightarrow {}^{223}Ra$	0.961	1.7
$^{228}Th \rightarrow {}^{224}Ra$	0.897	41

Discussion

Modelling the physico-chemical mechanisms for radionuclide supply and removal at the geothermal site in Bruchsal are based on the following assumptions: an isotropic system is assumed in which a large conductive fracture of width w_f and height h_f are intersected by microfractures. These microfractures are part of the rock matrix with a very low hydraulic conductivity, and thus, water flow is assumed to take place only in the fracture.

The flow rate is parallel to the fracture orientation with a fracture length L_f that coincides with the principal direction of groundwater flow. The fracture dimensions are assumed to be large relative to their aperture. Water–rock interactions take place in both regions, in the matrix blocks and in the fracture. However, the latter has a relatively low water–rock interaction rate due to their differences in surface area-to-fluid ratio. A schematic overview of the Bruchsal reservoir is shown in Fig. 9.

Since water–rock interaction rates occur at different timescales, their impact on U–Th series radionuclides varies depending on their half-lives. While mineral dissolution (leaching) mainly affects long-lived radionuclides, the physical process of alpha-recoil is mainly associated with short-lived nuclides (cf. Eq (17)).

Assuming that large fractures channel the geothermal brine and alpha-recoil directly into fractures is the only process adding radium into solution, the observed $^{224}Ra/^{228}Ra$ ratios should be greater than or equal to those in the rock material. However, ratios observed in the Bruchsal brine are lower (mean $^{224}Ra/^{228}Ra = 0.65$), indicating that alpha-recoil depends on half-lives of the respective radionuclides.

Alpha-recoil supply rates and recoil efficiencies

Modeling the radium supply from recoil (P_r), Eq. (19) is applied to the site-specific input parameter. Since the recoil efficiency is hard to determine, it might be estimated from ^{222}Rn activity in brine. Since ^{222}Rn is an inert gas, it is entirely dissolved and can therefore be measured directly. Its production is from alpha-recoil of ^{226}Ra that is within a recoil distance of ~ 40 nm of mineral surfaces as well as from the decay of the dissolved parent ^{226}Ra in brine. Therefore, mass balance for ^{222}Rn can be expressed as follows:

$$A_{222Rn} = P_{r,222Rn} + R_{f,226Ra} A_{226Ra}. \tag{36}$$

The fraction of ^{222}Rn atoms that is produced by alpha-recoil to its total fluid activity describes its recoil efficiency. Luo et al. (2000) proposed the following equation for calculating the ^{222}Rn recoil efficiency:

$$\varepsilon_{222} = \frac{P_{r,222Rn}}{A_{222Rn}} = \frac{1}{1 + \left(\left(\frac{\overline{A_{238U}}}{A_{232Th}} \right) \cdot \left(\frac{A_{224Ra}}{A_{228Ra}} - 1 \right) \cdot \left(\frac{A_{228Ra}}{A_{226Ra}} \right) \right)^{-1}}, \tag{37}$$

assuming that ratio of alpha-recoil supply for ^{222}Rn and ^{224}Ra equals the $^{238}U/^{232}Th$ activity ratio in rocks. According to that ^{222}Rn recoil efficiency (ε_{222}) is ca. 23% at the Bruchsal geothermal site, suggesting that the primary source of dissolved ^{222}Rn is ^{226}Ra decay dissolved in brine (rather than the ^{226}Ra decay in the solid phase). Krishnaswami et al. (1982) used ^{222}Rn to normalize recoil efficiency. They defined the recoil efficiency of nuclide i relative to the ^{222}Rn efficiency as a function of (a) its position in the decay chain and (b) on the adsorption behavior of its progenitor. An example is given for the daughter–parent couple of ^{224}Ra–^{228}Ra. Since both isotopes are members of the ^{232}Th decay chain, ^{224}Ra is closely related to ^{228}Ra. However, while ^{228}Ra is generated by a single alpha decay, ^{224}Ra is generated by two alpha decays (cf. Fig. 1). Thus, for ^{224}Ra the probability of recoiling into water is significantly larger than that for ^{228}Ra, resulting in a

higher recoil efficiency for ^{224}Ra relative to ^{228}Ra. Table 10 lists values of recoil efficiencies for radium as well as the recoil supply rates calculated from Eq. (19).

Diffusional flux

Since alpha-recoil supply is largest from surface areas with the highest contact areas, the recoil mechanism is most pronounced in the hydraulically inactive rock matrix. Rama and Moore (1984) suggested that diffusion along pore spaces and microfractures is believed to supply the recoiled atoms to the larger fractures where the sampled brine resides. Here, microfractures serve as diffusion pathways. The flux of radium into the large fracture fluid can be estimated from Eq. (38) as follows (Ku et al. 1992):

$$F_{Ra} = \phi^* \sqrt{\frac{D_m}{\lambda}} \left(P_r + R_f' A' - R_f A \right), \tag{38}$$

where Φ^* is the microfracture porosity, D_m is the molecular diffusivity of radium, λ is the decay constant, P_r is the supply rate from recoil (atoms kg^{-1} s^{-1}). R_f is the retardation factor and A is the activity of dissolved nuclide (atoms kg^{-1} s^{-1}) with superscript (′) referring to its radioactive parent.

Porosity is expected to be 0.05. The molecular diffusivity for radium at 135 °C is ca. 2.6×10^{-5} cm^2 s^{-1} calculated from the Stokes–Einstein relation (dynamic viscosity $\eta = 0.285 \times 10^{-3}$ Pa s; hydrodynamic Stokes radius for radium $R_{Ra} = 3.98$ Å). The term $R_f' A'$ is negligible since thorium progenitors are very insoluble in the geothermal system. The retardation factor of radium is assumed to be 1.3 estimated from the ^{222}Rn/^{226}Ra brine activity ratio (cf. Table 3).

Radium supply from recoil entering the fracture fluid does not only depend on diffusional flux, but also on the fracture width w_f, expressed as follows:

$$P_r^* = \frac{2F_{Ra}}{w_f}. \tag{39}$$

Applying Eq. (39) to radium with an estimated fracture width w_f of 10 mm (as stated in the GB2 drilling report) results in a significant fractionation of the Ra isotopes (Table 12). The diffusional flux of radium considering an effective diffusion length ($\phi^* \sqrt{D_m/\lambda}$) is listed in Table 11. Since the effective diffusion length depends on the decay constant λ, it varies between 0.2 cm for the shortest-lived ^{224}Ra and several tens of centimeter for the longest-lived ^{226}Ra in the geothermal brine. In consequence, the discharge flux density (atoms cm^{-2} s^{-1}) decreases with increasing decay constants limiting the ^{223}Ra and ^{224}Ra

Table 11 Model-derived rates of diffusional flux F_{Ra} as a function of the effective diffusion length ($\phi^* \sqrt{D_m/\lambda}$) for radium isotopes

Decay	$\phi^* \sqrt{D_m/\lambda}$ (cm)	F_{Ra} (atoms cm^{-2} s^{-1})
^{230}Th → ^{226}Ra	69	1.3×10^{-1}
^{232}Th → ^{228}Ra	4.2	2.9×10^{-2}
^{227}Th → ^{223}Ra	0.3	3.5×10^{-4}
^{228}Th → ^{224}Ra	0.2	5.3×10^{-3}

Table 12 Model-derived rate constants of adsorption (k_1) and desorption (k_2); dissolution (k_w) and precipitation (k_p) of radium and the related in situ retardation factors (R_f) due to sorption processes and (R_f^*) due to sorption processes as well as co-precipitation

Isotopes of Ra	$k_{1,Ra}$ (s^{-1})	$k_{2,Ra}$ (s^{-1})	$R_{f,Ra}$ ()	$k_{w,Ra}$ (s^{-1})	$k_{p,Ra}$ (s^{-1})	$R^*_{f,Ra}$()
^{226}Ra	6.0×10^{-10}	2.2×10^{-9}	1.3	2.3×10^{-8}	3.4×10^{-8}	2485
^{228}Ra			1.1			10
^{223}Ra			1.0			1.0
^{224}Ra			1.0			1.0

fluid activity (Table 11). These results are in line with the statement of Rama and Moore (1984) who pointed out that migration through microfractures may restrict the input of short-lived radionuclides because the rate of diffusion through microfractures is so slow that it reduces the effect of alpha-recoil supply. However, their study focused on the very short-lived ^{220}Rn, and thus, one may have some doubts if it is applicable to isotopes with longer half-lives.

Hammond et al. (1988), for example, suggest that radium reaches the large fractures within a few hours and thus, diffusional flux does not limit the activity of the short-lived Ra isotopes. Their study focused on the uranium and thorium series radionuclides in brines and reservoir rocks from two deep geothermal boreholes in the Salton Sea Geothermal Field (SSGF), California. From their modeling results, they postulated that the observed fluid activity of ^{223}Ra and ^{224}Ra can be explained by alpha-recoil, while only half of the ^{228}Ra and even less than 1% of the ^{226}Ra activity can be explained by alpha-reoil mechanisms. In consequence, the residual proportions of the ^{228}Ra and ^{226}Ra activities are contributed by weathering and leaching processes of radium from solid phases occurring on timescales comparable to the half-lives of ^{228}Ra and ^{226}Ra. Their approach is supported by an observed deficiency of ^{226}Ra in the SSFG reservoir section (Zukin et al. 1987).

However, in this study the situation is exactly opposite since the previous work of the authors figured out that ^{226}Ra is accumulated in the solids of the Bruchsal reservoir section suggesting that ^{226}Ra is rather removed from brine than leached from solids (Kölbel et al. 2020).

Ra removal by adsorption and precipitation

^{226}Ra can be removed from brine either by adsorption or by solid solution formation or both (Langmuir and Melchior 1985). Equal activities of ^{226}Ra and of its (unreactive) daughter ^{222}Rn indicate that ^{226}Ra is rarely adsorbed. Referring to Eq. (15) retardation factor is not only a function of k_1 and k_2, but is also dependent on the decay constant of the respective nuclide. Should the desorption rate constant k_2 be much greater than the decay constant of ^{224}Ra ($\lambda_{224Ra} = 2.209 \times 10^{-6}$ s^{-1}), then $R_{f,224Ra} = R_{f,223Ra} = R_{f,228Ra} = R_{f,226Ra}$ (Luo et al. 2000) applies. Otherwise short-lived radium isotopes will undergo less retardation than the long-lived ^{226}Ra due to their widely ranging half-lives.

Retardation factors for the short-lived radium isotopes might be calculated from the approach suggested by Krishnaswami (Eq. (22ff)). However, deviations in the $P/\lambda C$

ratio from unity might rather result from ^{224}Ra depletion in large fractures than from adsorption.

Therefore, only some general consideration about the retardation of radium could be made. Assuming that radium behaves mostly conservative (^{226}Ra/^{222}Rn = 1.3) and that the desorption rate constant is small compared to the ^{224}Ra decay constant which is likely because of the high radium solubility in the geothermal brine, short-lived ^{224}Ra should experience less retardation than ^{226}Ra ($R_{f,224Ra} \neq R_{f,226Ra}$). Hence, considering a min/max approach ($R_{f,min} = R_{f,224Ra} = 1.0$; $R_{f,max} = R_{f,226Ra} = 1.3$) with respect to the isotope half-lives, adsorption–desorption rates constants are in order of 10^{-10} s^{-1} for k_1 and 10^{-9} s^{-1} for k_2 (Table 12).

Previous studies of the adsorption behavior of radium in high-temperature and high-saline natural waters indicate that scavenging of radium by sorption processes might be of minor importance. Tanner (1964) proposed that during cation exchange Ra adsorption may be reduced because of the competition between radium and other alkaline earth metals for sorption sites resulting in an enrichment of radium in saline waters due to Ra-displacement from the rock surface by other cations with higher affinity to the exchange sites.

A rough estimate of the quantity of radium adsorbed on the rock surface may be calculated employing MIN3P. For calculations, an average cation exchange capacity (CEC) value of 2.00 meq/100 g was chosen since the reservoir material in Bruchsal mainly consists of quartz-dominated sandstones ($CEC_{quartz} = 0.6$ meq/100 g according to Carroll 1959). Thermodynamic data for cation exchange were taken from PHREEQC2-database (Parkhurst and Appelo 1999). With respect to the chemical composition of the Bruchsal brine (Table 1), radium competes with Na, K, Mg, Sr, Ba and Cs for cation exchange sites. The results show that the adsorbed radium species vary between 10^{-17} and 10^{-12} meq/100 g corresponding to radium distribution coefficients K_d of 0.014 to 0.016 mL g^{-1}.

However, these model-derived K_d values may differ from the in situ distribution coefficients. Thus, the control of radium activities by adsorption cannot yet be proven without further site-specific investigations regarding the chemical behavior of radium for different environmental conditions.

Should adsorption play a minor role, ^{226}Ra activity should be controlled by co-precipitation. Hammond et al. (1988) pointed out that the determination of first-order precipitation rate k_p (s^{-1}) and dissolution rate constants k_w (s^{-1}), respectively, may be obtained from solving simultaneously mass balance equations for radium isotopes. Combining Eq. (16) with Eqs. (18, 19, 25 and 26) and assuming $C^i = 0$, the mass balance equation for radium at steady state can be expressed as:

$$\overline{A'} e_i \varepsilon_{222} r S \rho_s + \frac{k_w \overline{A}}{\lambda} - \left(1 + \frac{k_p}{\lambda} + \frac{1}{\lambda \tau_b}\right) A = 0. \tag{40}$$

Simultaneous solution of Eq. (40) was performed for ^{226}Ra and ^{228}Ra, the two radium isotopes with half-lives in the order of years. The resulting rate constants are in the range of 10^{-8} s^{-1} for both, dissolution and precipitation, whereas k_p slightly exceeds k_w (Table 12).

From the calculated rate constants further information can be obtained about radium kinetics. Hammond et al. (1988) argued that the mean time for radium in solution equals the mass of radium in the solid phase divided by the flux into solution expressed as follows:

$$\tau_{w,Ra} = \frac{M_r}{M_b} \frac{\overline{A}}{\lambda C} \frac{1}{k_w}, \tag{41}$$

where M_b is the mass of brine and M_r is the mass of rock. Assuming a fracture porosity of 1% (since the ^{226}Ra accumulation in the reservoir rock was limited to fractured zones), the mean time for radium dissolution is predicted to be approximately 500 years. The mean time of radium in solution to precipitate in minerals $\left(\tau_{p,Ra} = 1/k_p\right)$ is estimated at circa 1 year.

The model-derived rates for dissolution (P_w) and precipitation (S_p) are listed in Table 12 demonstrating that radium will be preferred co-precipitate with minerals than leached from the solid phases.

Langmuir and Melchior (1985) found that the concentrations of dissolved radium in some deep brines in north Texas were likely to be controlled by co-precipitation in sulfate minerals due to the high concentrations of sulfate and earth-alkali ions. Barite is a typical sulfate mineral incorporating radium in solid solution as [Ba,Ra]SO_4. Both earth-alkali ions consist of an equal ionic charge and show similar ionic radii (radium = 1.52 Å, barium = 1.35 Å according to Shannon 1976). The observation by Langmuir and Melchior (1985) is confirmed by current studies dealing with the formation of Ra-bearing barite in German geothermal sites (Heberling et al. 2017; Haas-Nüesch et al. 2018).

From petrographic studies of the Bruchsal reservoir rock, it is known that barite often occurs in the reservoir section as a result of hydrothermal activities (Kölbel et al. 2020).

Zhen-Wu et al. (2016) studied barite dissolution and precipitation rates as a function of temperature and aqueous fluid composition. Their results demonstrate that barite readily achieves equilibrium with its adjacent fluid phase over a range of ionic strengths (aqueous NaCl concentrations = 0 to 1.5 molal) and in the presence of divalent metal cations (Ca, Mg and Sr) at temperatures ranging from 25 to 90 °C. They concluded that aqueous solution–barite equilibrium is broadly achieved in nature. Although reservoir temperature and molality of the NaCl geothermal brine are slightly increased compared to the experimental conditions (T = 134.7 °C; M(NaCl) = 2.1 mol kg^{-1}), rate constants for k_p and k_w presented by Zhen-Wu et al. (2016) are in the same order of magnitude as those derived by the mass balance approach. Consequently, Ra removal from brine by co-precipitation with barite might be a possible explanation for the ^{226}Ra anomaly observed in the Bruchsal geothermal reservoir.

Ra supply by groundwater flow

Assuming a water recharge in the Black Forest at the Eastern main border of the URG as suggested by several numerical models of coupled heat- and fluid-flow (e.g., Clauser and Villinger 1990), meteoric water infiltrates into the Permo-Triassic aquifer of the Rhinegraben. Since this infiltrating water is low in natural occurring radionuclides, the initial

Table 13 Model-derived production and scavenging rates (atoms kg^{-1} s^{-1}) for radium in the Bruchsal geothermal system

Water–rock interaction processes	^{226}Ra	^{228}Ra	^{223}Ra	^{224}Ra
Supply from alpha-recoil in consideration of the diffusional flux				
P_r^*	244	56	0.7	10
Production from desorption				
P_d	1268	1	0.0	0.0
Production from dissolution				
P_w	72,391	102	0.0	0.0
Scavenging from adsorption				
S_a	1276	2	0.0	0.0
Scavenging from precipitation				
S_p	72,585	141	0.0	0.0
Supply by water flow				
Q	−13	0.0	0.0	0.0
Steady-state activity				
A_{Ra}	29	16	0.7	10

concentration of radium can be assumed to be negligible ($C^i = 0$ atoms kg^{-1}). The water transit time τ_b is estimated at 5000 years (assuming a flow distance of $x = 5$ km and a fluid velocity $v_f = 1$ m $year^{-1}$). Calculation of Q by applying Eq. (18) results in negative values which indicate radium loss rather than radium supply due to mass transport in groundwater. However, Q is only notable for ^{226}Ra (cf. Table 13), since the rate of radium loss for ^{228}Ra, ^{223}Ra and ^{224}Ra is $\leq 2.6 \times 10^{-2}$ atoms kg^{-1} s^{-1}.

Steady-state Ra fluid activities

At steady state, the removal rates (activity of dissolved and adsorbed radium and precipitation) are equal to inputs (radium recoil rate and production from dissolved and absorbed Th progenitors), so that (Porcelli et al. 2014):

$$A_{Ra,steady} = \frac{P_r + P_w}{R_f + \left(\frac{k_p}{\lambda}\right)} = \frac{P_r + P_w}{R_f^*}. \tag{42}$$

Equation (42) might be used as a control for the discussed water–rock interactions since it merges the single interaction processes which should lead to the radium fluid activities measured in the Bruchsal brine. The denominator of the fraction reflects the retardation factor R_f^* due to precipitation as well as adsorption and desorption. Since R_f^* does not differ from R_f for short-lived radionuclides, R_f^* will increase with decreasing decay constants (Table 12).

Implications

Table 13 summarizes radium production and removal rates of the water–rock interaction processes discussed. From the results it becomes obvious that for ^{224}Ra and ^{223}Ra, precipitation and dissolution processes can be neglected and so removal by decay is

equal to inputs from recoil for ^{228}Th and ^{227}Th, respectively, within the solids for steady-state conditions. Consequently, alpha-recoil is the most important process for the short-lived ^{223}Ra and ^{224}Ra, to enter the fluid system.

On the other hand, it is interesting to note that not only ^{226}Ra, but also ^{228}Ra is affected by dissolution–precipitation processes. This is in line with the statement of Hammond et al. (1988) who postulated that these processes occur on timescales comparable to the half-lives of ^{228}Ra and ^{226}Ra. Furthermore, the authors' previous work has shown that in the Bruchsal reservoir fractured and hydrothermally altered horizons are associated with a preferential accumulation of ^{226}Ra in the solid phase caused by water–rock interaction between the hot geothermal fluid and the associated solid (Kölbel et al. 2020). Studying water–rock interaction processes may therefore support the detection of productive geothermal reservoir horizons, which is one of the major challenges in geothermal exploration.

Model-derived Ra steady-state activities are in good agreement with the observed Ra fluid activities (cf. Table 5) which support the applicability of the diffusional flux model. The diffusion of radium through microfractures do not only restrict the short-lived radionuclides as it is postulated by Rama and Moore (1984), but it has also a reinforcing effect on the ^{226}Ra activity due to its relatively high diffusional flux.

Conclusions

Even though naturally occurring radionuclides in geothermal brines can represent a challenge regarding the operational safety of a geothermal plant (there are currently some on-site research dealing with the use of inhibitors), they also can provide a supplementary tool for the characterization of geothermal reservoirs.

In this study, we investigated the behavior of U–Th series radionuclides in the brine of the Bruchsal geothermal site, located at the eastern main boundary of the Upper Rhine Graben (Germany). Permo-Triassic sedimentary rocks, affected by large-scale normal faults, host the geothermal reservoir.

Isotopes of Ra (^{226}Ra, ^{228}Ra, ^{224}Ra, ^{223}Ra), Rn (^{222}Rn) and Pb (^{210}Pb, ^{212}Pb), U (^{238}U, ^{234}U, ^{235}U), Th (^{232}Th, ^{228}Th, ^{230}Th), Po (^{210}Po) and Ac (^{227}Ac, ^{228}Ac) were analyzed over a sampling period from October 2016 to May 2017. The results show discrepancies between the fluid activities of the Th–U series nuclides measured in the Bruchsal brine: while isotopes of U, Th, Ac and Po are below the limit of analytical determination ($< 10^{-2}$ Bq kg^{-1}), isotopes of Rn (^{222}Rn = 38 Bq kg^{-1}), Ra (^{226}Ra = 29 Bq kg^{-1}; ^{228}Ra = 16 Bq kg^{-1}; ^{224}Ra = 11 Bq kg^{-1}; ^{223}Ra = 0.5 Bq kg^{-1}) and Pb (^{210}Pb = 26 Bq kg^{-1}; ^{212}Pb = 16 Bq kg^{-1}) are rather soluble.

Differences in chemical and physical properties result in radioactive disequilibria. Modeling the disequilibria based on radium (^{226}Ra, ^{228}Ra, ^{224}Ra, ^{223}Ra) enabled us to estimate rate constants of water–rock interactions. Since the daughter–parent ratio of ^{222}Rn/^{226}Ra is ca. 1.3, Ra retardation due to sorption processes is small resulting in adsorption–desorption rate constants in the range of 10^{-10} s^{-1} for k_1 and 10^{-9} s^{-1} for k_2. Model-derived Ra distribution coefficients K_d vary between 0.014 and 0.016 mL g^{-1}. First-order precipitation rate constant ($k_p = 3.4 \times 10^{-8}$ s^{-1}) slightly exceeds those of dissolution ($k_w = 1.2 \times 10^{-8}$ s^{-1}). Precipitation occurs on timescales comparable to ^{226}Ra

and ^{228}Ra, while the short-lived ^{224}Ra and ^{223}Ra ($t_{1/2}$ = 3.66 and 11.43 days, respectively) are not affected. Indeed, the short-lived Ra isotopes are mostly supplied from alpha-recoil.

Assuming a fracture porosity of 1%, the average time to leach all ^{226}Ra ($=M_r\, A_r\, \lambda^{-1}$) from solid phases is predicted at ca. 500 years, while the average time of dissolved radium to co-precipitate in minerals is estimated at circa 1 year.

Since fractured zones provide a substantial portion of the permeability due to the low porosity of the Bruchsal sandstone reservoir rock, the observed decay-series disequilibria in brine can best be explained by the following conclusions on water–rock interaction processes:

(1) The hydraulically inactive pore spaces and microfractures, respectively, are the main source for alpha-recoil, while recoil supply from large fractures may be negligible due to their relative low brine-rock interaction rates.
(2) Diffusional flux through pore spaces and microfractures is believed to supply radionuclides to the large conductive fractures causing a significant fractionation of Ra isotopes.
(3) Migration through microfractures may limit input of short-lived Ra isotopes into solution, depending on isotope half-lives and fracture geometry.
(4) Radium removal is rather by co-precipitation with solid solutions than by sorption processes which is indicated by the isotopic ratio of ^{222}Rn/^{226}Ra = 1.3 in brine.
(5) Co-precipitation of radium is most likely for barite and restricted to the fractured reservoir section.

From (1) and (2) it can be concluded that the recoil input is strongly diffusion-controlled which might be used to gain information about the fracture surface area (Andrews et al. 1989). For the short-lived ^{223}Ra and ^{224}Ra, alpha-recoil is the most important process to enter the fluid system. Thus, the activity of ^{223}Ra (^{224}Ra) dissolved within the large fracture fluid depends on the diffusional flux from rock surfaces and the size of the fracture. Estimates about the specific surface area ($m^2\ m^{-3}$) may be deduced from the known flux (F_{Ra}) and the fluid activity (A_{Ra}) of the radium isotopes. In this case, the specific surface area is defined as the surface area of solids per volume of fracture fluid contacting the solids (which corresponds to the flow-wetted surface area). Since the specific surface area of the fracture is inversely proportional to the fracture width, further information about the site-specific fracture geometry can be obtained. However, it should be noted that this fracture width represents an averaged equivalent aperture since the fluid samples analyzed are mostly collected from the larger aperture, hydraulically conductive fractures. Thus, the fracture surface area depends on (1) whether the estimated fracture width represents one large or several smaller fractures and (2) the extent of the variance from the averaged equivalent fracture width. With regard to reservoir engineering, it might be interesting to solve this question in more detail. Based on the determination of the averaged equivalent aperture, additional numerical modelling of heat transfer is a promising option to solve these questions.

Acknowledgements
We are grateful to the laboratory of IAF (Dresden) that performed the alpha-ray measurements and the laboratory of EnBW Kernkraft GmbH where the gamma spectrometry surveys were carried out. We especially thank G. Gkogkidis for

his great support in setting up the gamma spectrometric measuring stations. Careful reviews by anonymous reviewers greatly improved the manuscript. In addition, we acknowledge support by the Open Access Publication Funds of the Göttingen University.

Authors' contributions
All authors had a hand in the preparation of the manuscript and the interpretation of the data. All authors read and approved the final manuscript.

Funding
This research was carried out within the framework of the ANEMONA project, funded by the German Federal Ministry for Economic Affairs and Energy (BMWi). Open access funding provided by Projekt DEAL.

Availability of data and materials
The data used to support the findings of this study are included within the article.

Competing interests
The authors declare that they have no competing interests.

Author details
[1] Department of Applied Geology, Geoscience Centre, University of Göttingen, Goldschmidtstr. 3, 37077 Göttingen, Germany. [2] Research and Innovation Department, EnBW Energie Baden-Württemberg AG, Durlacher Allee 93, 76131 Karlsruhe, Germany. [3] Department of Applied Geology, Institute of Geosciences, Friedrich-Schiller-University Jena, Burgweg 11, 07749 Jena, Germany.

Received: 9 July 2020 Accepted: 21 August 2020
Published online: 08 September 2020

References

Allison JD, Brown DS, Novo-Gradac KJ. MINTEQA2/PRODEFA2; A geochemical assessment model for environmental systems, version 3.0, users's manual, EPA/600/3-91/021, Environ. Res. Lab., U.S. Environ. Prot. Agency, Washington, D. C. 1991.

Andrews JN, Giles IS, Kay RLF, Lee DJ, Osmond JK, Cowart JB, Fritz P, Barker JF, Gale J. Radioelements, radiogenic helium and age relationships for groundwaters from the granites at Stripa, Sweden. Geochim Cosmochim Acta. 1982;46:1533–43.

Andrews JN, Ford DJ, Hussain N, Trevedi D, Youngman MJ. Natural radioelement solution by circulating groundwaters in the Stripa granite. Geochimica et. Cosmochimica Acta. 1989;53:1791–802.

Attendorn HG, Bowen RNC. Radioactive and Stable Isotope Geology. London: Chapman and Hall; 1997. p. 522.

Bateman H. Solution of a system of differential equations occurring in the theory of radioactive transformations. Proceed Cambr Philos Soc. 1910;15:423–7.

Beaucaire C, Criaud A, Michard G. Contrôle des concentrations de certains éléments traces (As, Sb, U, Ra, Ba) dans les eaux du Cézallier (Massif Central, France). Chem Geol. 1987;63:85–99.

Carroll D. Ion exchange in clays and other minerals. Geol Soc Am Bull. 1959;70:749–80.

Clauser C, Villinger H. Analysis of conductive and convective heat transfer in a sedimentary basin, demonstration for the Rheingraben. Geophys J Int. 1990;100:393–414.

Condomines M, Rihs S, Lloret E, Seidel JL. Determination of the four natural Ra isotopes in thermal waters by gamma-ray spectrometry. Appl Radiat Isot. 2010;68:384–91.

Condomines M, Gourdin E, Gataniou D, Seidel J-L. Geochemical behaviour of Radium isotopes and Radon in a coastal thermal system (Balaruc-les-Bains, South of France). Geochim Cosmochim Acta. 2012;98:160–76.

Davidson MR, Dickson BL. A porous flow model for steady-state transport of radium in ground waters. Water Resour Res. 1986;22:34–44.

Degering D, Köhler M. Gamma-spectrometric analysis of high salinity fluids—how to analyze radionuclides of the thorium decay chain far from radioactive equilibrium? Appl Radiat Isot. 2011;69:1613–7.

Dickson BL. Radium isotopes in saline seepage, southwestern Yilgarn, Western Australia. Geochim Cosmochim Acta. 1985;49:349–60.

Eggeling L, Genter A, Kölbel T, Münch W. Impact of natural radionuclides on geothermal exploitation in the Upper Rhine Graben. Geothermics. 2013;47:80–8.

Foster DA, Staubwasser M, Henderson GM. ^{226}Ra and Ba concentrations in the Ross Sea measured with multicollector ICP mass spectrometry. Mar Chem. 2004;87:59–71.

Gascoyne M. Geochemistry of the actinides and their daughters. In: Ivanovich M, Harmon RS, editors. Uranium-Series Disequilibrium Applications to Earth, Marine, and Environmental Sciences. Oxford: Clarendon Press; 1992. p. 34–61.

Grandia F, Merino J, Bruno J. Assessment of the radium-barium co-precipitation and its potential influence on the solubility of Ra in the near-field Stockholm, Swedish Nuclear Fuel and Waste Management Co: 2008; 52.

Grundl T, Cape M. Geochemical factors controlling radium activity in a sandstone aquifer. Ground Water. 2006;44–4:518–27.

Haas-Nüesch R, Heberling F, Schild D, Rothe J, Dardenne K, Jähnichen S, Eiche E, Marquardt C, Metz V, Schäfer T. Mineralogical characterization of scalings formed in geothermal sites in the Upper Rhine Graben before and after the application of sulfate inhibitors. Geothermics. 2018;71:264–73.

Hammond DE, Zukin JG, Ku TL. The kinetics of radioisotope exchange between brine and rock in a geothermal system. J Geophys Res. 1988;93(13):175–86.

Heap MJ, Villeneuve M, Kushnir ARL, Farquharson JI, Baud P, Reuschlé T. Rock mass strength and elastic modulus of the Buntsandstein: an important lithostratigraphic unit for geothermal exploitation in the Upper Rhine Graben. Geothermics. 2019;77:236–56.
Heberling F, Schild D, Degering D, Schäfer T. How well suited are current thermodynamic models to predict or interpret the composition of (Ba, Sr)SO4 solid-solutions in geothermal scalings? Geotherm Energy. 2017;5(1):9.
Jerez-Vegueria SF, Godoy JM, Miekeley N. Environmental impact studies of barium and radium discharges by produced waters from the "Bacia de Campos" oil-field offshore platforms, Brazil. J Environ Radioact. 2002;62:29–38.
Joachim H, Koziorowski G, Leiber J. Geothermiebohrungen Bruchsal 1a und 2. In: Maus H, editor. Jahreshefte des Geologischen Landesamtes Baden-Württemberg 29. Freiburg i. Br.: Herder; 1987. p. 84–97.
Kigoshi K. Alpha recoil ^{234}Th: dissolution in water and the ^{234}U/^{238}U disequilibrium in nature. Science. 1971;173:47–8.
Kraemer TF, Reid DF. The occurrence and behavior of radium in saline formation water of the U.S, Gulf Coast region. Isotope Geosci. 1984;2:153–74.
Krishnaswami S, Graustein WC, Turekian KK, Dowd JF. Radium, thorium and radioactive lead isotopes in groundwaters: applications to the in situ determination of adsorption-desorption rate constants and retardation factors. Water Resour Res. 1982;18(6):1633–75.
Kölbel L, Kölbel T, Wiegand B, Sauter M, Schäfer T, Siefert D. Identification of fractured zones in geothermal reservoirs in sedimentary basins: a radionuclide-based approach. Geothermics. 2020;85:101764.
Ku T-L, Luo S, Leslie BW, Hammond DE. Decay-series disequilibria applied to the study of water-rock interaction and geothermal systems. In: Ivanovich M, Harmon RS, editors. Uranium-series Disequilibrium: Applications to Earth, Marine, and Environmental Sciences. Oxford: Clarendon Press; 1992. p. 631–68.
Ku TL, Luo S, Leslie BW, Hammond DE. Assessing in situ radionuclide migration from natural analog studies: response to McKinley and Alexander (1996). Radiochim Acta. 1998;80:219–23.
Langmuir D, Melchior D. The geochemistry of Ca, Sr, Ba, and Ra sulfates in some deep brines from the Palo Duro Basin, Texas. Geochim Cosmochim Acta. 1985;49:2423–32.
Lasaga AC. Kinetic Theory in the Earth Sciences. Princeton: Princeton Univ Press; 1998.
Luo S, Ku T-L, Roback R, Murrell M, McLing TL. In-situ radionuclide transport and preferential groundwater flows at INEEL (Idaho): decay-series disequilibrium studies. Geochim Cosmochim Acta. 2000;64:867–81.
Mao S, Duan Z. The P, V, T, x properties of binary aqueous chloride solutions up to T = 573 K and 100 MPa. J Chem Thermodynamics. 2008;40:1046–63.
Mayer KU, Frind EO, Blowes DW. Multicomponent reactive transport modeling in variably saturated porous media using a generalized formulation for kinetically controlled reactions. Water Resour Res. 2002;38:1174.
Moise T, Starinsky A, Katz A, Kolodny Y. Ra isotopes and Rn in brines and ground waters of the Jordan-Dead Sea Rift Valley: enrichment, retardation, and mixing. Geochim Cosmochim Acta. 2000;64–14(2371):2388.
Moore WS. High fluxes of radium and barium from the mouth of the Ganges Brahmaputra River during low river discharge suggest a large groundwater source. Earth Planetary Sci Lett. 1997;150:141–50.
Nozaki Y, Yamamoto Y, Manaka T, Amakawa H, Snidvongs A. Dissolved barium and radium isotopes in the Chao Phraya River estuarine mixing zone in Thailand. Cont Shelf Res. 2001;21:1435–48.
Osmond JK, Cowart JB. Ground water. In: Ivanovich M, Harmon RS, editors. Uranium-series Disequilibrium: Applications to Earth, Marine, and Environmental Sciences. Oxford: Oxford Science Publications; 1992. p. 290.
Parkhurst DL, Appelo CAJ. User's guide to PHREEQC–A computer program for speciation, reaction-path, 1D-transport, and inverse geochemical calculations: Technical Report 99–4259. Survey Water-Resources Investigations Report: US Geol; 1999.
Parkhurst DL, Appelo CAJ. Description of Input and Examples for PHREEQC Version 3-A Computer program for speciation, batch-reaction, one-dimensional transport, and inverse geochemical calculations. US: Department of the Interior, U.S. Geological Survey; 2013.
Porcelli D. Investigating groundwater processes using U- and Th-series nuclides. In: Baxter MS, editor. Radioactivity in the Environment 13. Amsterdam: Elsevier; 2008. p. 105–53.
Porcelli D, Kim C-K, Martin P, Moore WS, Phaneuf M. Properties of radium, In: IAEA (Ed.), the environmental behavior of radium (revised edition), technical report series no. 476, Vienna, 2014; 6-32.
Pribnow D, Schellschmidt R. Thermal tracking of upper crustal fluid flow in the Rhine Graben. Geophys Res Lett. 2000;27:1957–60.
Rama, Moore WS. Mechanism of transport of U-Th series radioisotopes from solids into ground water. Geochim Cosmochim Acta. 1984;48:395–400.
Rihs S, Condomines M, Sigmarsson O. U, Ra and Ba incorporation during precipitation of hydrothermal carbonates: implications for 226Ra-Ba dating of impure travertines. Geochim Cosmochim Acta. 2000;64:661–71.
Rihs S, Condomines M. An improved method for Ra isotope (^{226}Ra, ^{228}Ra, ^{224}Ra) measurements by gamma spectrometry in natural waters: applications to CO_2-rich thermal waters from the French Massif Central. Chem Geol. 2002;182:409–21.
Rodriguez-Galan RM, Prieto M. Interaction of nonideal, multicomponent solid solutions with water: a simple algorithm to estimate final equilibrium states. Geochem Geophys Geosyst. 2018;19:1348–59.
Shannon RD. Revised effective ionic radii and systematic studies of interatomic distances in halides and chalcogenides. Acta Crystallogr A. 1976;32:751–67.
Sturchio N, Bohlke J, Markun F. Radium geochemistry of geothermal waters, Yellowstone National Park, Wyoming, USA. Geochimica et Cosmochimica Acta. 1993;57:1203–14.
Sturchio N, Banner J, Binz C, Heraty L, Musgrove M. Radium geochemistry of ground waters in Paleozoic carbonate aquifers, mid-continent, USA. Appl Geochem. 2001;16:109–22.
Sun H, Semkow T. Mobilization of thorium, radium and radon radionuclides in ground water by successive alpha-recoil. J Hydrol. 1998;205:126–36.
Tanner AB. Radon migration in the ground: a review. In: Adams JAS and Lowder WM (eds), The Natural Radiation Environment, Chicago, 1964; 161–190.

Tricca A, Porcelli D, Wasserburg GJ. 2000. Factors controlling the ground water transport of U, Th, Ra, and Rn. Proceedings of the Indian Academy of Sciences, 109, 95–108.
Tricca A, Wasserburg GJ, Porcelli D, Baskaran M. The transport of U- and Th-series nuclides in a sandy unconfined aquifer. Geochim Cosmochim Acta. 2001;65:1187–210.
Zhen-Wu BY, Dideriksen K, Olsson J, Raahauge PJ, Stipp SL, Oelkers EH. Experimental determination of barite dissolution and precipitation rates as a function of temperature and aqueous fluid composition. Geochim Cosmochim Acta. 2016;194:193–210.
Ziegler PA. European Cenozoic rift system. Tectonophysics. 1992;208:91–111.
Zukin JG, Hammond DE, Ku T-L, Elders WA. Uranium-Thorium series radionuclides in brines and reservoir rocks from two deep geothermal boreholes in the Salton Sea geothermal field, southeastern California. Geochim Cosmochim Acta. 1987;51:2719–31.

Publisher's Note